

Special  
Issue

# 1,2,4-Oxadiazole Topsentin Analogs with Antiproliferative Activity against Pancreatic Cancer Cells, Targeting GSK3 $\beta$ Kinase

Daniela Carbone<sup>+</sup>,<sup>[a, b]</sup> Barbara Parrino<sup>+</sup>,<sup>[a]</sup> Stella Cascioferro,<sup>[a]</sup> Camilla Pecoraro,<sup>[a, b]</sup> Elisa Giovannetti,<sup>[b, c]</sup> Veronica Di Sarno,<sup>[d]</sup> Simona Musella,<sup>[d]</sup> Giulia Auriemma,<sup>[d]</sup> Girolamo Cirrincione,<sup>[a]</sup> and Patrizia Diana<sup>\*[a]</sup>

A new series of topsentin analogs, in which the central imidazole ring of the natural lead was replaced by a 1,2,4-oxadiazole moiety, was efficiently synthesized. All derivatives were pre-screened for antiproliferative activity against the National Cancer Institute (NCI-60) cell lines panel. The five most potent compounds were further investigated in various pancreatic ductal adenocarcinoma (PDAC) cell lines, including SUIT-2, Capan-1, and Panc-1 cells, eliciting EC<sub>50</sub> values in the micromolar and sub-micromolar range, associated with significant reduction of cell migration. These remarkable results might be explained by the effects of these new topsentin analogues on epithelial-to-mesenchymal transition markers, including SNAIL-

1/2 and metalloproteinase-9. Moreover, flow cytometric analysis after Annexin V-FITC and propidium iodide staining demonstrated that these derivatives enhanced apoptosis of PDAC cells. Keeping with these data, the PathScan intracellular signaling and ELISA array revealed cleavage of caspase-3 and PARP and a significant inhibition of GSK3 $\beta$  phosphorylation, suggesting this kinase as a potential downstream target of our novel compounds. This was further supported by a specific assay for the evaluation of GSK3 $\beta$  activity, showing IC<sub>50</sub> values for the most active compounds against this enzyme in the micromolar range.

## 1. Introduction

A huge number of new compounds used in drug regimens for the treatment of different cancer types, have been obtained directly or indirectly from natural sources, modifying the molecular structure of natural compounds or synthesizing new derivatives using their structures as models. Among the small-

molecule approved drugs for all diseases in the last 30 years, only the 17% are considered as merely synthetic, being the 83% natural products *per se* or mimicked natural products.<sup>[1]</sup>

Different anticancer agents have been isolated from marine sources that offered unique secondary metabolites with significant biological activities. In particular, more than half of the new marine natural products discovered from 1985 to 2012 showed anticancer properties and among these, several molecules were approved or tested in clinical trials.<sup>[2]</sup> Examples of marine-derived approved drugs are represented by trabectedin, a tetrahydroisoquinoline alkaloid first isolated from the ascidian *Ecteinascidia* approved by the European Union (EU) in 2007 and by the Food and Drug Administration (FDA, US) in 2015 for the treatment of adult patients with advanced soft tissue sarcoma, and eribulin mesylate, a synthetic analog of halichondrin B isolated from marine sponges, that was approved by the FDA in 2010 and by the EU in 2011 for patients with locally advanced or metastatic breast cancer.<sup>[2]</sup>

Considering the success gained by molecules derived from the marine environment, our research group synthesized a library of compounds obtained through the structure manipulation of nortopsentin, a natural bis-indolyl alkaloid isolated from deep-sea sponge *Spongosorites ruetzleri* which is characterized by significant antiproliferative activity against the P388 murine leukemia cell line.<sup>[3]</sup> In particular, we produced many derivatives in which the central imidazole ring was replaced by several five-membered heterocycles.<sup>[4-7]</sup>

Successively, structural manipulation of nortopsentins involved an indole moiety, which was modified into an azaindole portion and many derivatives showed significant antiprolifer-

[a] Dr. D. Carbone,<sup>+</sup> Dr. B. Parrino,<sup>+</sup> Dr. S. Cascioferro, C. Pecoraro, Prof. G. Cirrincione, Prof. P. Diana  
Department of Biological, Chemical and Pharmaceutical Sciences and Technologies (STEBICEF)  
University of Palermo  
Via Archirafi 32  
90123, Palermo (Italy)  
E-mail: patrizia.diana@unipa.it

[b] Dr. D. Carbone,<sup>+</sup> C. Pecoraro, Prof. E. Giovannetti  
Department of Medical Oncology  
VU University Medical Center (VUmc)  
De Boelelaan 1117  
1081HV, Amsterdam (The Netherlands)

[c] Prof. E. Giovannetti  
Cancer Pharmacology Lab, AIRC Start Up  
Fondazione Pisana per la Scienza  
Via Ferruccio Giovannini 13  
56017 San Giuliano Terme, Pisa (Italy)

[d] Dr. V. Di Sarno, Dr. S. Musella, Dr. G. Auriemma  
Department of Pharmacy  
University of Salerno  
Via G. Paolo II 132  
84084 Fisciano (Italy)

[\*] These authors contributed equally to this work.

Supporting information for this article is available on the WWW under <https://doi.org/10.1002/cmdc.202000752>

This article belongs to the Special Collection "NMMC 2019: DCF-SCI 40th Anniversary"

ative activity in a wide range of human tumor cell lines.<sup>[8–10]</sup> Some of them acted as CDK1 inhibitors,<sup>[11–12]</sup> and the most active derivatives determined a significant reduction of tumor volume with two complete responses at well-tolerated doses in mesothelioma mouse models.<sup>[13]</sup>

These promising results prompted us to perform additional studies, focusing our attention on the bis-indolyl alkaloid topsentins, characterized by the presence of a carbonyl group that differentiates their skeleton from that of the nortopsentin, as linker between one of the two indolyl portion and the position 2 of the central imidazole ring. Topsentin and bromotopsentin (Figure 1) were extracted from the sponge *Topsentia genitrix*. Topsentin showed *in vitro* cytotoxic activity against P-388 murine tumor cells, with IC<sub>50</sub> value of 8.8 μM and against several human tumor cells, including HCT-8, A-549, T47D. In addition, it exhibited *in vivo* activity against P-388 (T/C 137%, 150 mg/kg) and B16 melanoma (T/C 144%, 37.5 mg/kg). Bromotopsentin was found to be active against human non-small-cell bronchopulmonary cancer cells NSCLC–N6 and P-388, with IC<sub>50</sub> values of 28.5 μM and 16.6 μM, respectively.<sup>[14,15]</sup>

Deoxytopsentin, bromodeoxytopsentin and isobromodeoxytopsentin (Figure 1) are also belonging to the topsentin class, and were isolated from *Hexadella sp.* and *Spongosorites genitrix* sponges, respectively. The unsubstituted deoxytopsentin was found to be active against human lung cancer (NSCLC–N6), breast cancer (BC) and hepatoma (HepG2) cells, reporting IC<sub>50</sub> values of 19.3, 32.8 and 10.1 μM, respectively. Bromodeoxytopsentin and isobromodeoxytopsentin showed cytotoxicity against the human leukemia cell-line K-562, with LC<sub>50</sub> values of 1.5 and 5.2 μM, respectively.<sup>[16,17]</sup>

On the other hand, nitrogen heterocycles constitute the pharmacophore moiety of several molecules with different biological activities,<sup>[18–20]</sup> including antitumor activity.<sup>[21–24]</sup> These compounds are able to improve the interaction with target proteins, enzymes and receptors through the formation of hydrogen bonds, dipole-dipole and hydrophobic interactions, van der Waals forces and π-stacking interactions. Moreover, the presence of the nitrogen atom allows to improve solubility.<sup>[25]</sup> Among nitrogen heterocycles, the 1,2,4-oxadiazole ring is found in many molecules with significant biological activity, especially antitumor<sup>[26–29]</sup> and being a bioisostere of amides and esters is

able to improve bioavailability and physicochemical properties of compounds bearing it.

Considering the interesting antiproliferative activity of topsentins, as well as the important features and properties of the 1,2,4-oxadiazole ring, herein we report the synthesis of the new 1,2,4-oxadiazole topsentin analogs **1** (Figure 1). The biological activity of the synthesized compound was investigated against the NCI-60 panel and on cell lines of pancreatic ductal adenocarcinoma, one of the most aggressive solid malignancies characterized by poor response to current treatments and extremely poor prognosis.

## 2. Results and Discussion

### 2.1. Chemistry

We successfully synthesized the new 1,2,4-oxadiazoles of type **1** following a multistep sequence described in Scheme 1. The retrosynthetic analysis of the title ring system suggested N-hydroxy-1*H*-indole-3-carboxamide **2**, and (1-methyl-1*H*-indol-3-yl)-oxo-acetic acid **3** as suitable building blocks.

The N-hydroxy-1*H*-indole-3-carboxamides **2a–d** (75–85%) were synthesized from 1*H*-indole-3-carbonitriles **4a–d**, prepared from the corresponding indoles **5a–d**, as previously reported,<sup>[30,31]</sup> through reaction with hydroxylamine hydrochloride in ethanol (EtOH), in the presence of diisopropylethylamine (DIPEA).

The (1-methyl-1*H*-indol-3-yl)-oxo-acetic acids (**3a–d**) were prepared from the commercially available 1*H*-indoles **5** which were subjected to methylation, providing the corresponding methyl derivatives **6**.<sup>[7,12,32]</sup> Their subsequent acylation using an excess of oxalyl chloride in diethyl ether, at 0°C and under nitrogen atmosphere, gave **7a–d** in excellent yields (89–96%).

In the attempt to obtain 1,2,4-oxadiazoles **1**, compounds **7** were first reacted with carboxamides of type **2**. In spite of several reaction conditions employed, in no case, the expected compounds were isolated in acceptable yields, due to the extreme reactivity of the indolyl-oxo-acetyl chlorides in the complex reaction mixture. Thus, acyl chlorides were converted into oxo-acetic acids **3a–d** (78–95%), using a solution of sodium

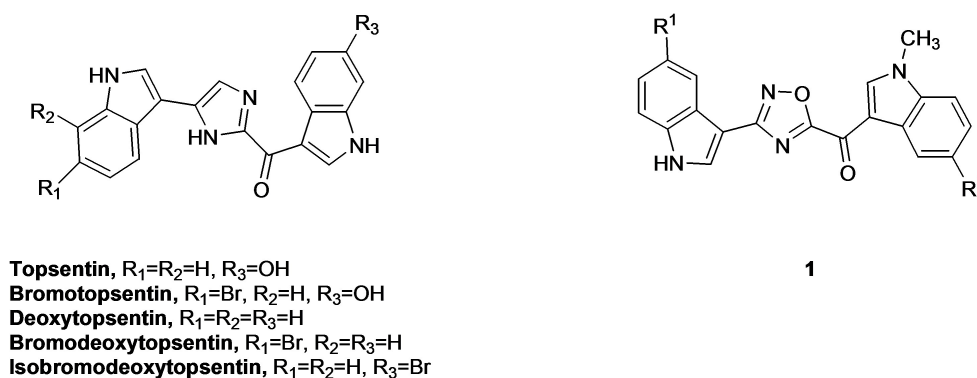
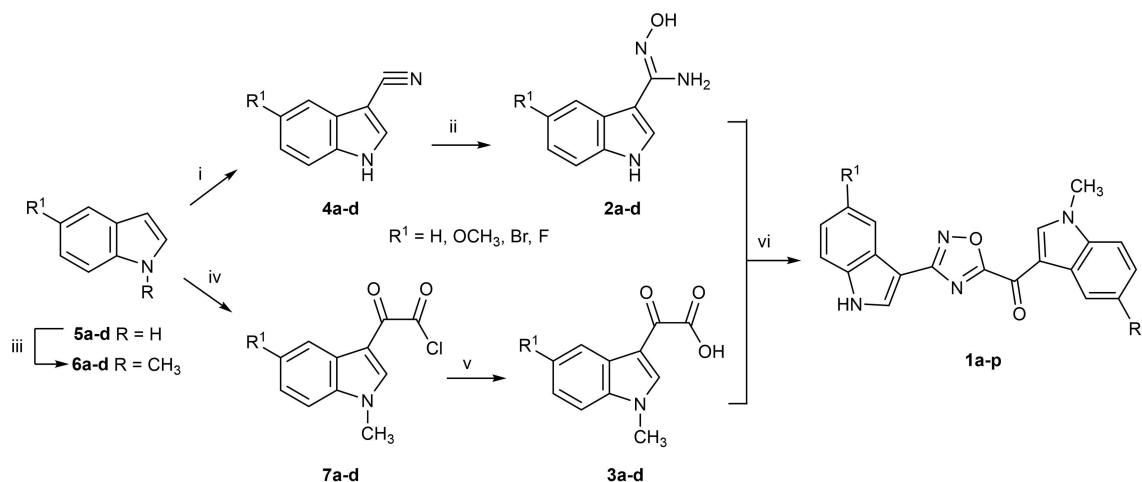


Figure 1. Structures of topsentins and new topsentin analogs **1**.



**Scheme 1.** Synthesis of [3-(1*H*-Indol-3-yl)-1,2,4-oxadiazol-5-yl](1-methyl-1*H*-indol-3-yl)methanone **1a–p**. Reagents and conditions: (i) (a) CSI, MeCN, 0 °C, 2 h; (b) DMF, 0 °C, 1 h, 90–98%; (ii) NH<sub>2</sub>NH<sub>2</sub> HCl, DIPEA, EtOH, reflux, 4 h, 75–85%; (iii) *t*-BuOK, TDA-1, toluene, RT, 1–24 h, then CH<sub>3</sub>l, RT, 1–2 h, 97–99%; (iv) oxalyl chloride, diethyl ether, 0 °C, 3 h, then 24 °C, 1 h, 89–96%; (v) NaOH 2 M, THF, RT, 12 h, 78–95%; (vi) EDC, HOBT, DMF, 0 °C, 15 min, then 100 °C, 15 min, 45–78%.

hydroxide (NaOH) at room temperature. The reaction between the two key building blocks **2a–d** and **3a–d** was performed in DMF and in the presence of *N*-(3-dimethylaminopropyl)-*N*'-ethylcarbodiimide hydrochloride (EDC) and hydroxybenzotriazole (HOBT) as the coupling reagents, inducing the formation of an amide bond by previous activation of the carboxylic acid group.<sup>[33]</sup> Subsequent *in situ* temperature-catalyzed cyclodehydration, performed warming the reaction mixture at 100 °C, gave the desired oxadiazole derivatives **1a–p** in yields ranging from 45–78%.

## 2.2. Biology

### 2.2.1. Antiproliferative activity

According to the NCI protocol, all the newly synthesized oxadiazoles **1a–p** were screened for *in vitro* antiproliferative activity in a panel of 60 human tumor cell lines derived from 9 human cancer cell types, grouped in disease sub-panels (supporting information, Table S1). The growth percentages were calculated and the “One-dose” (10 μM) data was reported as a mean graph of the percent growth of treated cells. Among all submitted oxadiazoles, the compounds **1b**, **1c** and **1l** showed the best mean growth percentages, with growth inhibition values, against several cancer cell lines, lower than 10%. In particular, the compound **1b** showed a high level of tumor selectivity, exhibiting pronounced lethality toward cell lines derived from melanoma (MDA-MB-435, –19.13%) and leukemia (HL-60, –6.73%). The cell lines OVCAR-3 (ovarian cancer), HT29 (colon cancer) and NCI–H522 (non-small cell lung cancer) were also highly sensitive to the antiproliferative effects of this drug (growth values, 0.72%, 8.80% and 2.36%, respectively) (Table S1). For the compound **1c**, the strongest activity was detected toward melanoma MDA-MB-435 (7.96%), as well as against breast MDA-MB-468 (–4.38%) cells (Table S1).

The same data mining approach from the NCI-60 panel demonstrated that the most sensitive cell lines for the compound **1l** were SR (included in the leukemia subpanel), SW-620 (colorectal cancer), OVCAR-4 (ovarian cancer) and DU-145 (prostate cancer), with growth percent values of 6.41%, –2.17%, –0.34 and 3.08%, respectively (Table S1).

Since the NCI panel do not include PDAC cell lines, we decided to evaluate the *in vitro* antiproliferative activity of these compounds on a panel of immortalized PDAC cells, including SUIT-2, Capan-1 and Panc-1, by Sulforhodamine-B (SRB) assay. These analyses allowed us to get further insight about the drug activity of our compounds against additional cancer cell models. Furthermore, the search for novel effective drugs is extremely important in PDAC, a devastating type of cancer with poor survival rates due to very limited therapeutic options.

An initial screening was performed using three concentrations (0.1 μM, 1 μM, 10 μM). Below, data of compounds **1b**, **1c**, **1i**, **1j** and **1l**, which showed significant cytotoxic activity, were reported (Figure 2).

In particular, the compounds **1b** and **1c** were more active against the SUIT-2 pancreatic cells, if compared to the other cells, with mean growth percent values of 18.97% and 27.09%, respectively (Figure 2a,b). Conversely, the compounds **1i** and **1j** had highest antiproliferative/cytotoxic effects against CAPAN-1 cells, for which we observed growth percent values of –5.62% and 19.63%, respectively (Figure 2c,d). However, the compound **1l** at concentration of 10 μM inhibited the viability of all the three cell lines, with effects ranging from –0.04 to 34.31 percent of growth (Figure 2e).

To assess the potential toxicity effects of the new compounds **1b**, **1c**, **1i**, **1j** and **1l**, *in vitro* cell viability of immortalized human pancreatic normal ductal cells HPNE was measured after treatment with three different concentrations of each compound (0.1, 1 and 10 μM). As shown in the Figure 2f, all derivatives did not cause cytotoxic effects on non-tumor pancreatic cells. We found only 10–20% growth inhibition after

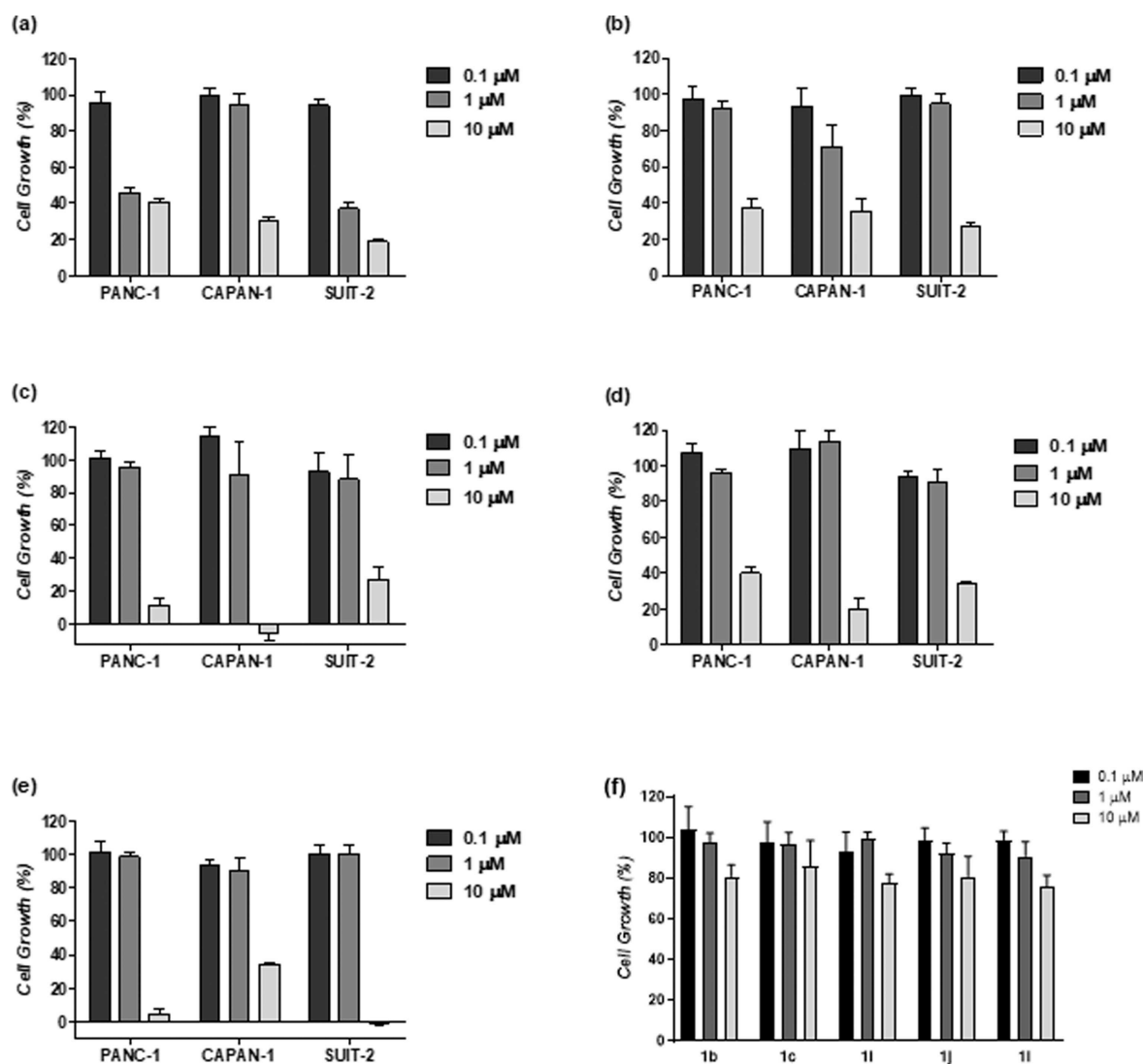


**Figure 2.** Cell growth data after 72 h exposure to the compounds **1b** (a), **1c** (b), **1i** (c), **1j** (d) and **1l** (e) using a panel of pancreatic cancer cell lines, as assessed by the SRB assay. In the panel (f), assessment of toxicity of compounds **1b**, **1c**, **1i**, **1j** and **1l** at three different concentrations against HPNE human normal pancreatic cells. The results are expressed as percentage of cell growth compared to untreated control cells. Columns, mean values obtained from three independent experiments; bars, SEM.

72 h of HPNE cells treated with the highest concentration tested (10  $\mu\text{M}$ ). The other concentrations tested (0.1 and 1  $\mu\text{M}$ ) did not impair the viability of HPNE cells. The results of these experiments allowed us to consider these new compounds highly cancer selective compared to the non-tumor pancreatic cells HPNE.

In order to better determine the concentration achieving a 50% inhibition ( $\text{EC}_{50}$ ) of cell growth, the PDAC cells were then exposed to nine increasing concentrations (from 0.1  $\mu\text{M}$  to 40  $\mu\text{M}$ ) of each compound for 72 hours. These studies revealed (Figure 3a,b) that SUIT-2 cells were the most sensitive cells to **1b**, with an  $\text{EC}_{50}$  value below 0.50  $\mu\text{M}$  (0.40  $\mu\text{M}$ ). This compound showed antitumor activity also against Panc-1 and Capan-1 cells, but with slightly higher  $\text{EC}_{50}$  values (0.8 and 1.2  $\mu\text{M}$ , respectively). Conversely the compound **1c** showed a lower anti-proliferative potency in SUIT-2 cells ( $\text{EC}_{50}$  = 3.2  $\mu\text{M}$ , Table 1),

**Table 1.** Summary of the antiproliferative activity of oxadiazole derivatives in pancreatic cancer cells.

Compound	$\text{EC}_{50}$ [ $\mu\text{M}$ ] <sup>[a]</sup>	Panc-1	Capan-1	SUIT-2
<b>1b</b>	0.8	1.2	0.40	
<b>1c</b>	1.6	1.3	3.2	
<b>1i</b>	2.8	2.8	7.1	
<b>1j</b>	6.8	2.6	5.9	
<b>1l</b>	1.5	1.4	1.9	
<b>Gemcitabine</b>	0.10	0.020	0.010	
<b>5-Fluorouracil</b>	4.3	0.50	0.91	

[a] Data are reported as  $\text{EC}_{50}$  values (the molar concentration of a compound where 50% of its maximal effect is observed) determined by the SRB assay after 72 hours exposure to each compound. Gemcitabine and 5-fluorouracil were reported as reference drugs. Data represent mean values from at least 3 independent experiments.

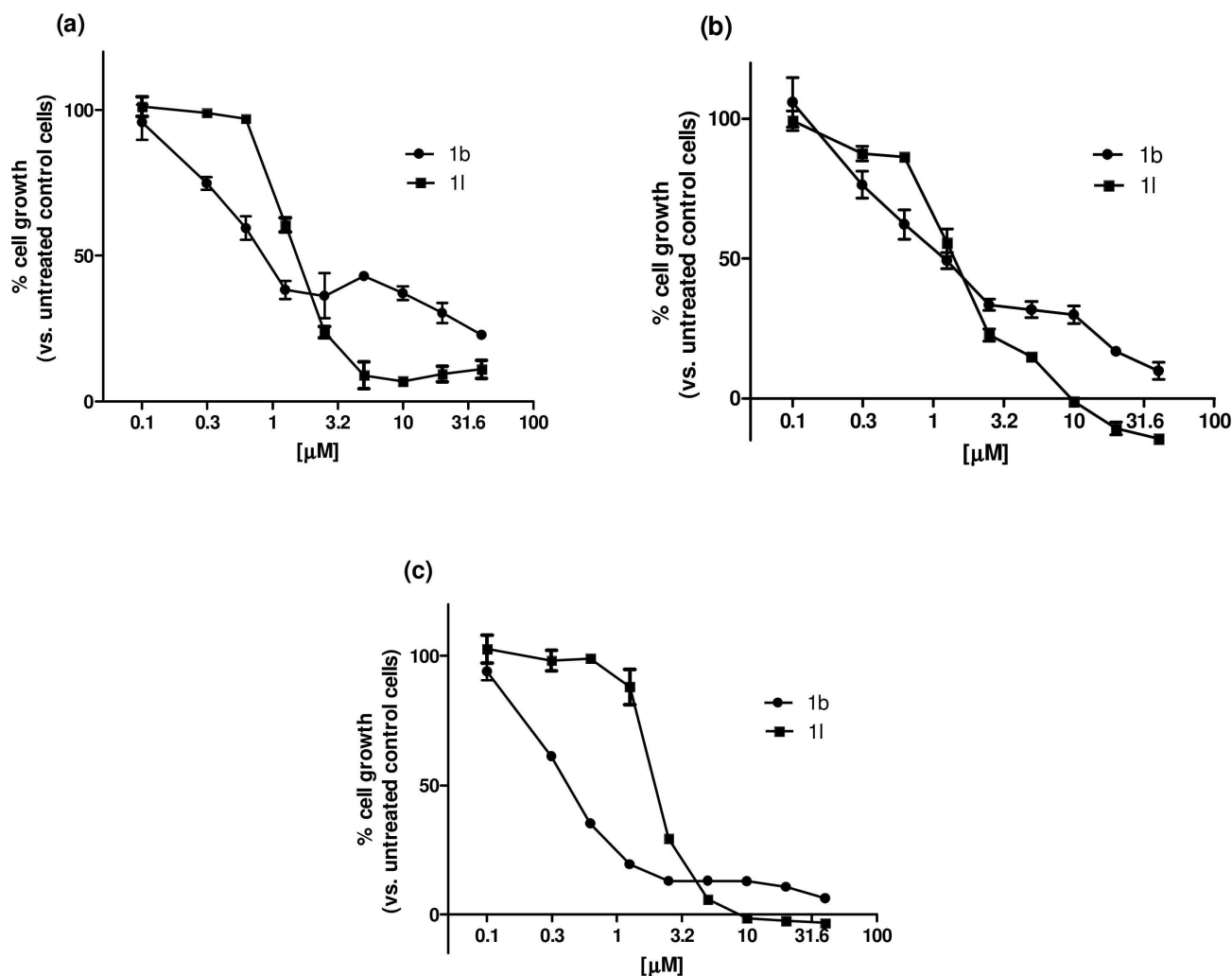


**Figure 3.** Effects of most active compounds **1b** and **1i** on the viability of Panc-1 (a), Capan-1 (b) and SUIT-2 (c) PDAC cell lines. Cells were treated with nine different concentrations of the compound and cell survival was measured after 72 h by SRB assay in comparison to untreated control cells. Values are reported as the mean  $\pm$  SEM of three separate experiments, performed in triplicate.

inhibiting the growth of Panc-1 and Capan-1 with  $IC_{50}$  values of 1.6 and 1.3  $\mu$ M, respectively. Similarly, the compound **1i** was more active against Panc-1 and Capan-1 cancer cell lines, with the same  $EC_{50}$  values of 2.8  $\mu$ M; while a weak antiproliferative activity was observed against SUIT-2 cell line (Table 1). The compound **1j** had  $EC_{50}$  values at higher micromolar levels, ranging from 2.6  $\mu$ M to 6.8  $\mu$ M (Table 1). However, the compound **1i** showed comparable antiproliferative activity against Panc-1, Capan-1 and SUIT-2 cells, with  $EC_{50}$  values of 1.5  $\mu$ M, 1.4  $\mu$ M and 1.9  $\mu$ M, respectively (Figure 3a-c).

Overall, it is clear that all derivatives resulted active from nanomolar to micromolar concentrations, against all of tested cell lines, as it has been confirmed by the range of  $EC_{50}$  values, from 0.40 to 7.1  $\mu$ M (Table 1).

### 2.2.2. Effects on cell-cycle modulation

Alterations in the cell cycle caused by **1b**, **1c** and **1i** were evaluated in the SUIT-2 cell line, which was selected because of the faster doubling time. Cell cycle progression was analyzed by cytofluorimetry, using propidium iodide (3,8-diamino-5-[3-(diethylmethylammonio)propyl]-6phenyl- diiodide, PI) staining solution.

In SUIT-2 cells, the compound **1b**, at concentration of 2  $\mu$ M and 5  $\mu$ M, decreased the G<sub>0</sub>/G<sub>1</sub> phase from 50.6% to 37.9% and 33.5%, respectively, as well as the S phase from 24.5% to 17.3% and 15.5%. In contrast, the G<sub>2</sub>/M phase increased from 24.9% to 44.8% and 51.0%. This could be due to the triggering, in at least some cell subpopulations, of different cell survival mechanisms in response to the antiproliferative effect of this compound, eventually leading to an increase in the number of mitosis events. The cells treated with **1i**, at both 5 and 10  $\mu$ M, gave results comparable to the ones obtained from the control samples, while all the samples treated with the compound **1c**

at 2  $\mu\text{M}$  and at 5  $\mu\text{M}$ , showed a reduction in the percentages of G<sub>0</sub>/G<sub>1</sub> cells to 32.6% and 30.4%, respectively. Conversely, the percentages of cells in the S-phase increased till 30.8% and 33.6%, respectively, while the G<sub>2</sub>/M phase increased to 36.6% after treatment with the compound **1c** at both 5 and 10  $\mu\text{M}$  (Figure 4).

### 2.2.3. Effects on induction of apoptosis

To prove the pro-apoptotic nature of new oxadiazole compounds against pancreatic cancer cells, an evaluation of externalization of plasma membrane phosphatidylserine, a reliable marker of cell apoptosis, was performed by flow cytometry analysis of annexin V-FITC and 7-Amino-Actinomycin D (7-AAD) stained cancer cells.

As shown in Figure 5a, the highest levels of apoptosis features were detectable after SUIT-2 cells were treated with

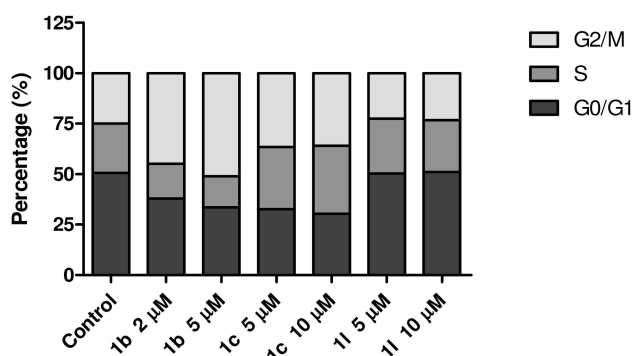


**Figure 4.** Effects of the oxadiazole compounds **1b**, **1c** and **1l** on cell cycle modulation. SUIT-2 cells were exposed for 24 hours and columns show the mean percentages of cells at various stages of cell cycle, G<sub>0</sub>/G<sub>1</sub> (black), S (dark gray), and G<sub>2</sub>/M (light gray) phase, in untreated control and after treatment with the compounds.

5  $\mu\text{M}$  or 10  $\mu\text{M}$  of **1l** for 24 hours. The apoptotic rates of SUIT-2 cells were increased in a concentration-dependent manner. In particular, the percentages of apoptotic SUIT-2 cells were 12.6% and 15.9% when compared to the control group (5.4%), when treated with 5  $\mu\text{M}$  and 10  $\mu\text{M}$  of the compound **1l**, respectively. The compound **1c** did also increase apoptotic death to 8.5% and 10.6% at 5  $\mu\text{M}$  and 10  $\mu\text{M}$ , respectively.

Induction of apoptotic death following treatment with **1c** and **1l** suggests that these compounds may orchestrate a potential modulation of the pathways that induce apoptosis, and we performed further studies in the Panc-1, which are mesenchymal pancreatic cancer cells. Compared to control cells (6.2%), the compound **1c**, at 5  $\mu\text{M}$  and 10  $\mu\text{M}$ , increased the apoptotic rate to 19.2% and 19.7%, respectively. The same effect was observed after treatment with **1l**, that increased the apoptotic rate to 18.2 and 19.0% at concentration of 5 and 10  $\mu\text{M}$  (Figure 5). Of note, the compound **1b** did not appreciably induce apoptotic death in both SUIT-2 and Panc-1 cells (data not shown).

### 2.2.4. Anti-migratory activity

In order to evaluate the impact of the compounds **1b**, **1c**, **1i**, **1j**, and **1l** on cell migration, which constitutes an important step in the metastatic process, the *in vitro* scratch wound healing assay has been performed on Capan-1, Panc-1 and SUIT-2 PDAC cell lines. The Panc-1 cell line was chosen for anti-migration study due to previous studies showing its highly aggressive and strongly metastatic properties.<sup>[34]</sup> However, further studies were performed in Capan-1 and SUIT-2 which are both derived from liver metastases of PDAC.

The compound **1b**, tested at concentrations of 2  $\mu\text{M}$  and 5  $\mu\text{M}$ , determined a slight inhibition of the migration rate of SUIT-2 and Panc-1 cells compared with untreated cells, 20 hours after the treatment (Table 2). On the other hand, the same

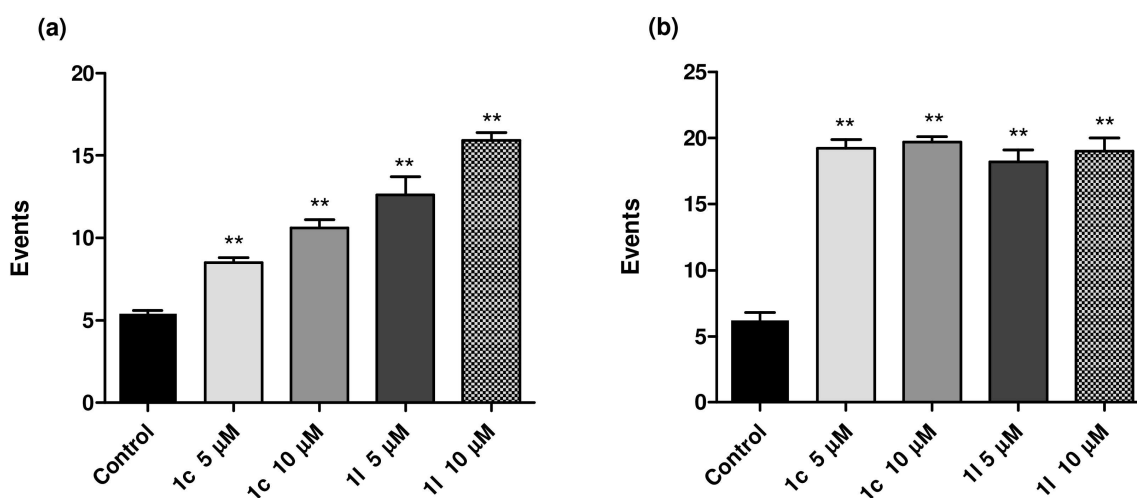


**Figure 5.** Effects of compounds **1c**, and **1l** on apoptosis induction in SUIT-2 (a) and Panc-1 (b) pancreatic cancer cells. The percentage of cells with apoptotic features was assessed by FACS analysis of annexin V after 24-hour treatment. Columns, mean values obtained from three independent measurements; bars, SEM; \*\* $P < 0.001$  compared to control/untreated cells.

**Table 2.** Percentages of migration monitored over time (0, 4, 8, 20 and 24 h) of Capan-1, Panc-1 and SUI-2 cells treated with the compounds **1 b**, **1 c**, **1 i**, **1 j** and **1 l**.

	Percentages of migration [%]											
	Capan-1 hours				Panc-1 hours				SUIT-2 hours			
	4	8	20	24	4	8	20	24	4	8	20	24
<b>Control</b>	34	43	87	95	29	34	86	95	4	8	17	20
<b>1 b 2 <math>\mu</math>M</b>	34	35	56	62	28	36	66	77	4	12	13	16
<b>1 b 5 <math>\mu</math>M</b>	34	36	49	56	25	29	73	81	3	8	12	13
<b>Control</b>	24	37	90	93	56	80	85	75	49	49	58	58
<b>1 c 5 <math>\mu</math>M</b>	26	34	68	80	40	61	65	77	51	49	62	62
<b>1 c 10 <math>\mu</math>M</b>	28	29	45	43	45	54	65	61	41	34	60	60
<b>Control</b>	30	5	95	100	20	35	57	67	32	47	51	57
<b>1 i 2 <math>\mu</math>M</b>	35	63	100	100	30	50	74	130	18	25	51	48
<b>1 i 5 <math>\mu</math>M</b>	38	71	100	100	40	42	71	133	24	31	54	48
<b>Control</b>	22	44	100	100	50	54	55	52	37	41	54	52
<b>1 j 5 <math>\mu</math>M</b>	35	57	100	100	50	67	66	56	41	41	53	60
<b>1 j 10 <math>\mu</math>M</b>	39	56	100	100	60	63	66	56	18	27	52	54
<b>Control</b>	34	34	100	100	20	32	91	96	4	6	7	20
<b>1 l 5 <math>\mu</math>M</b>	30	32	92	99	18	30	91	93	7	9	17	21
<b>1 l 10 <math>\mu</math>M</b>	27	31	86	94	14	27	84	92	7	9	14	16

compound, at both above-mentioned concentrations, showed strong inhibitory effects on the migration of Capan-1 cells (Figure 6). These effects were already detectable after 8 hours, as shown by the representative images in the Figure 6c, demonstrating that the cell density in the scratch area was reduced after treatment as reflected by a higher scratch area in treated wells (Figure 6b), compared to untreated/control wells. As reported in the Figure 6a, after 24 hours, the compound **1 b**, reduced the cell migration to 33% and 39%; at the concentration of 2  $\mu$ M and 5  $\mu$ M, respectively. The compound **1 c** had minimal effects on SUI-2, while a 20% decrease of migration was observed in Panc-1 cells between 8 and 20 hours after treatment (Table 2). However, this compound showed the best results in inhibiting the migration of Capan-1 cells, as reflected by a significantly higher scratch area in treated wells. In particular, after 20 h exposure, an average of 90% of the scratches was closed in the untreated wells, whereas after treatment at 5  $\mu$ M, only 45% of the scratches were closed (Table 2).

The compound **1 i** did not exhibit considerable inhibitory effect on cell migration. Conversely, the wound closure rate of SUI-2 cells was notably decreased when treated with 10  $\mu$ M of compound **1 j** at 4 h (18%) and 8 h (27%), compared with untreated/control SUI-2 cells (37% and 41%, respectively). However, no significant differences in the levels of cell migration were identified for the cells treated with the compound **1 j** at 5  $\mu$ M. The treatment of Panc-1 and Capan-1 cells with the same compound did not significantly modify the percentages of cell migration with respect to control (Table 2). Similarly, the treatment with the compound **1 l** at two concentrations (5  $\mu$ M and 10  $\mu$ M) in the assays performed on SUI-2, Panc-1 and Capan-1 cells was not able to stop the cells from healing the scratch wound.

### 2.2.5. Gene expression profiling of key factors in epithelial-mesenchymal transition and evaluation of MMP9 activity

Epithelial-mesenchymal transition (EMT) has been proposed as the critical mechanism for the acquisition of malignant phenotypes by epithelial cancer cells, resulting in tumour invasion and induction of the metastasis process.<sup>[35,36]</sup>

During EMT, primary site epithelial cells acquire the motile and invasive characteristics of mesenchymal cells, such as motility, invasiveness, and resistance to apoptosis, resulting in secondary tumor formation at another site.<sup>[37]</sup> Thus, controlling of EMT is considered a promising approach for the inhibition of metastasis.

In order to evaluate the capability of the most promising antitumor compounds (**1 b** and **1 l**) to modulate EMT, we firstly evaluated the effects on EMT critical determinants, such as SNAIL1, SNAIL2 and MMP9. To this goal, a specific Real-Time PCR analysis has been performed on the total mRNA extracted from the Panc-1 and Capan-1 PDAC cell lines.

Output data of the Real-Time PCR experiment (Figure 7) have been normalized by a standard curve of the housekeeping gene  $\beta$ -actin, in order to obtain quantitative information about gene expression levels, in Panc-1 and Capan-1 cells treated with the compounds **1 b** and **1 l**, at concentrations of 2  $\mu$ M and 5  $\mu$ M, compared to untreated control cells

Our correlation analysis indicated an interesting potential influence of the new topsentin analogues treatment on EMT pathways. In Panc-1 cells, both compounds **1 b** and **1 l** induced over-expression of SNAIL2 and MMP9 and down-regulation of SNAIL1 (Figure 7a). Similarly, in Capan-1 cells, the compounds **1 b** and **1 l** induced over-expression of SNAIL2 and MMP9. However, SNAIL1 expression was up-regulated under **1 b** treat-

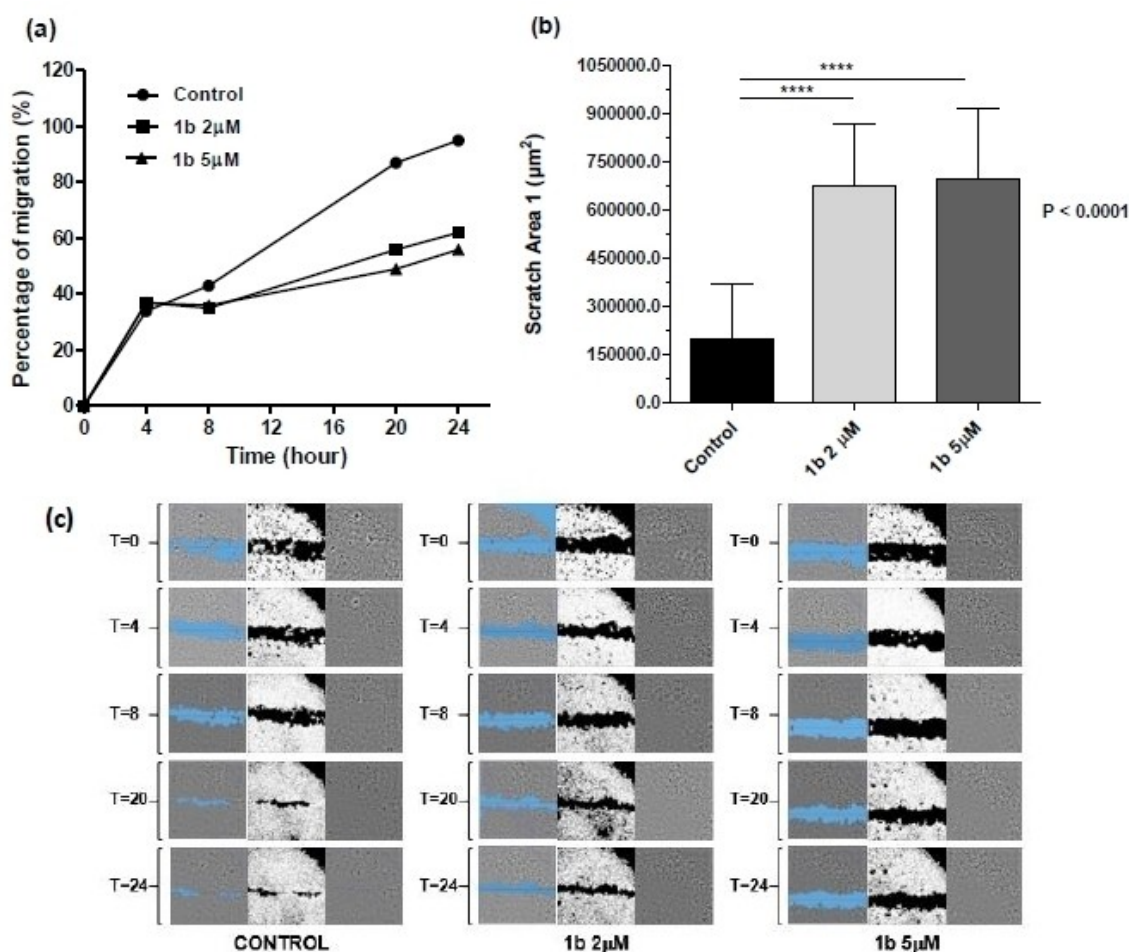


**Figure 6.** Evaluation of cell migration using the wound healing scratch assay. (a) The percentages of migration were calculated for untreated cells (control, circles), cells treated with **1b** at concentration of 2 µM (squares) and cells treated with **1b** at concentration of 5 µM (triangles). (b) Scratch area values and comparison of the areas of the scratches in Capan-1, calculated 20 hours after scratch and treatment with the compound **1b**. Columns, mean values; bars, SEM; \*\*\*\* $P < 0.0001$  compared to control/untreated cells (c) Representative images from wound healing assay of Capan-1 cell cultures treated with or without the compound **1b** at concentration of 2 µM and 5 µM.

ment. Conversely this expression was down-regulated under **11** treatment at 2 µM and up-regulated at 5 µM (Figure 7b).

These studies indicated that, regardless of cell phenotype, SNAIL2 mRNA was significantly over-expressed after treatment with our analogues. As reported in previous studies, we hypothesized the existence of a negative feed-back control by the protein SNAIL2, which might be a potential downstream molecular target of these compounds, and then could provide cells with the capability of buffering, meaning to stabilize SNAIL2 levels in spite of small perturbations.<sup>[38]</sup> Similarly, the gene of MMP-9 was over-expressed after treatment in both cell lines, suggesting a negative feed-back mechanism that controls MMP-9 mRNA expression. Through a specific gelatine zymography assay we indeed observed a decrease in the activity of MMP-9 protein levels (Figure 8), supporting the anti-migration activity induced by these compounds. In particular, our studies showed a significant decrease of the activity of MMP-9 isolated from Panc-1 and Capan-1 cells, which decreased by about 40% after 24 hours exposure to both compounds at 5 µM.

### 2.2.6. Modulation of key oncogenic signaling by protein phosphorylation array and ELISA

A protein phosphorylation array was performed on lysates of Panc-1 cells treated with the selected compounds (**1b** and **11**) to assess the phosphorylation or cleavage of an array of important proteins in oncogenic intracellular signaling (Figure 9a). The relative fluorescent units (RFU) were compared between the treatment conditions. We observed a significant decreased phosphorylation in the following proteins and phosphorylation sites: ERK1/2 Thr202/204, Bad Ser112 and GSK3β Ser9. Besides phosphorylation, we also assessed cleavage of caspase-3 and PARP which were associated with the induction of apoptosis, as described above. In order to validate whether our compounds could reduce GSK3β phosphorylation at serine residue 9 as well as at tyrosine 216, which are essential for the kinase activity of this protein we then performed specific ELISA assays. These assays were carried out on Panc-1 cells treated with compounds at concentrations of 5 µM for 24 hours.

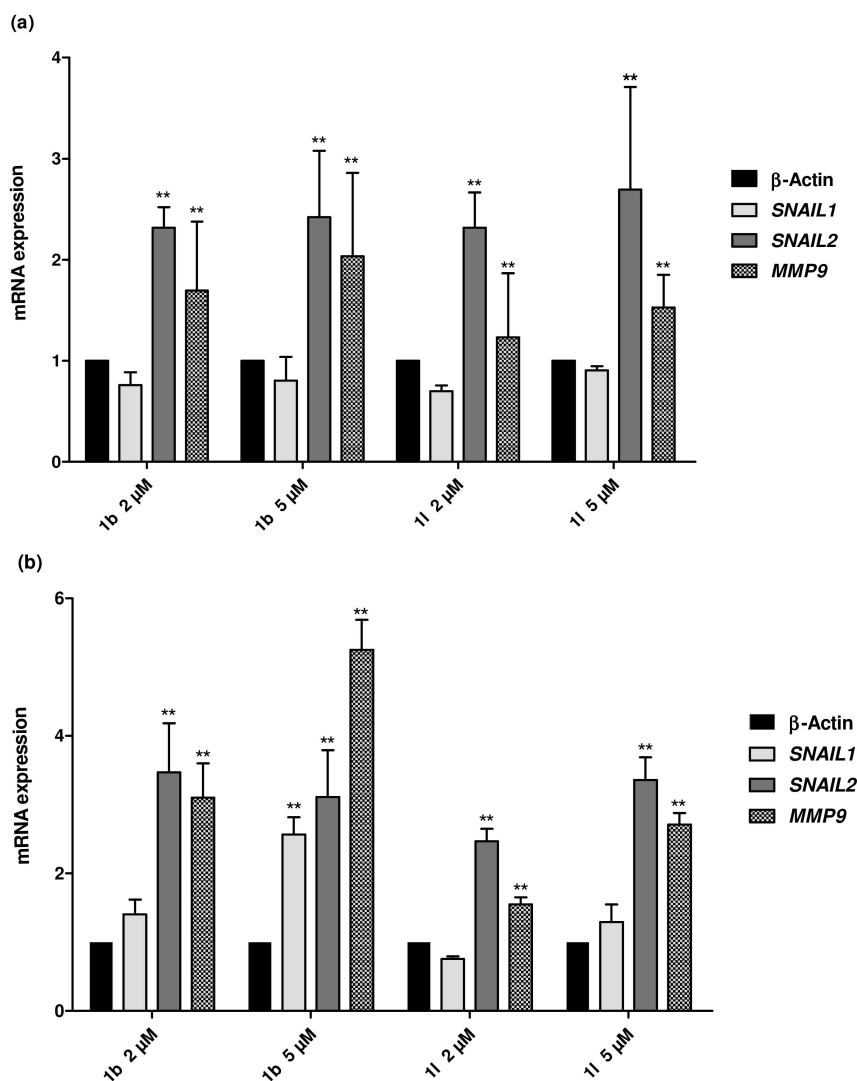


**Figure 7.** Analysis of the relative levels of SNAIL1, SNAIL2, and MMP9 gene expression by real-time quantitative PCR in Panc-1 (a) and Capan-1 (b) pancreatic cancer cells treated with the compounds 1b and 11, at concentration of 2  $\mu$ M or 5  $\mu$ M, for 24 hours. Normalized gene expression levels were given as the ratio between the mean value for the target gene and that of the housekeeping genes  $\beta$ -actin in each sample, compared to untreated/control cells whose expression values were set at 1; Columns, mean values; bars, SEM; \*\* $P < 0.001$  compared to control/untreated cells.

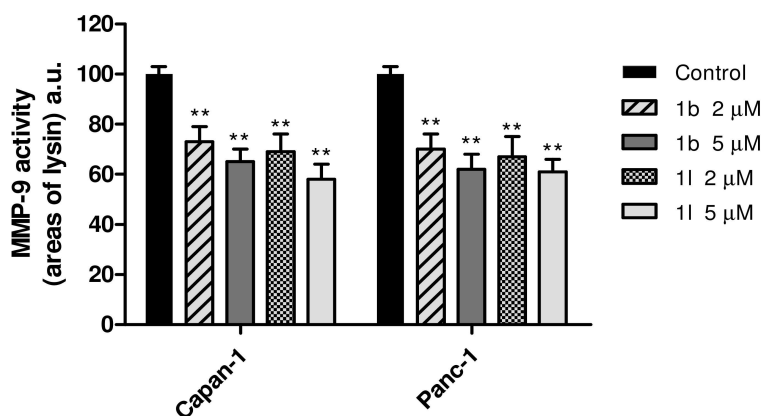


**Figure 8.** Gelatine zymography analysis of media from Capan-1 and Panc-1 cells incubated with serum-free medium for 24 hours. The enzymatic activity of MMP9 was determined by densitometric analysis. The cells were treated with the compounds 1b and 11 at concentration  $IC_{50}$  and  $2x IC_{50}$  values for 24 hours. Columns, mean values; bars, SEM; \*\* $P < 0.001$  compared to control/untreated cells.

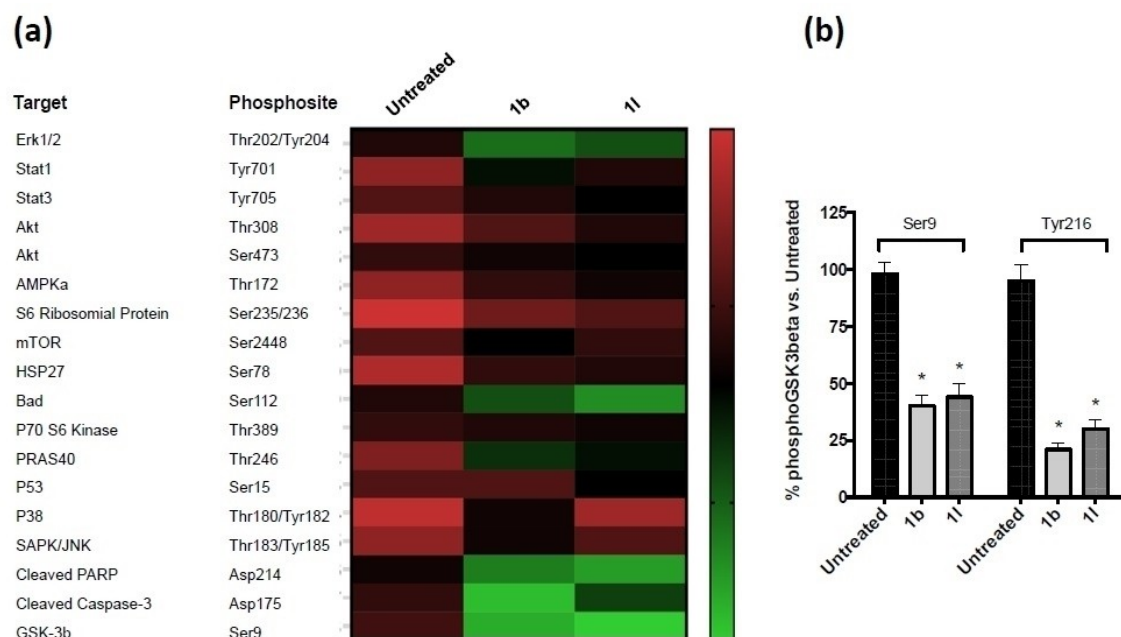


**Figure 9.** Modulation of key oncogenic signaling by protein phosphorylation array and ELISA. (a) Modulation of the phosphorylation or cleavage of an array of important proteins in oncogenic intracellular signaling. Red signals indicate higher phosphorylation levels, and green signals indicate lower phosphorylation levels. (b) Inhibition of GSK3 $\beta$  phosphorylation by compounds **1b** and **1I**. Modulation of phosphorylated-GSK3 $\beta$  (pGSK3 $\beta$ ) at serine residue 9 and at tyrosine residue 216 by compounds **1b** and **1I** in Panc-1 cells. Columns, mean values; bars, SEM; \* $P < 0.05$ .

As shown in the Figure 9b, we observed a reduction of phospho-GSK3 $\beta$  at serine residue 9 ranging from 40% to 50%, while the inhibition of phospho-GSK3 $\beta$  at tyrosine residue 216 ranged between 70 and 80%. Similar results were observed using the known inhibitor enzastaurin (data not shown). These results suggest that GSK3 $\beta$  is a target of our compounds and might explain how they can then suppress GSK3 $\beta$ -driven proliferation, anti-apoptotic and migration activities.

### 2.2.7. Kinase activity assays and molecular modelling

To further investigate whether our compounds could modulate the activity of GSK-3 $\beta$ , a specific ADP-Glo™ activity assay was employed. As shown in Figure 10a, the novel 1,2,4-oxadiazole compounds exhibited inhibition on GSK-3 $\beta$  in a dose-dependent manner. The concentrations leading to a loss of 50% enzyme activity ( $IC_{50}$ ) for the two most active compounds (**1b** and **1I**) were 0.62 and 0.81  $\mu$ M, respectively. The other compounds (**1c**, **1i** and **1j**) inhibited GSK3 $\beta$ , with a slightly

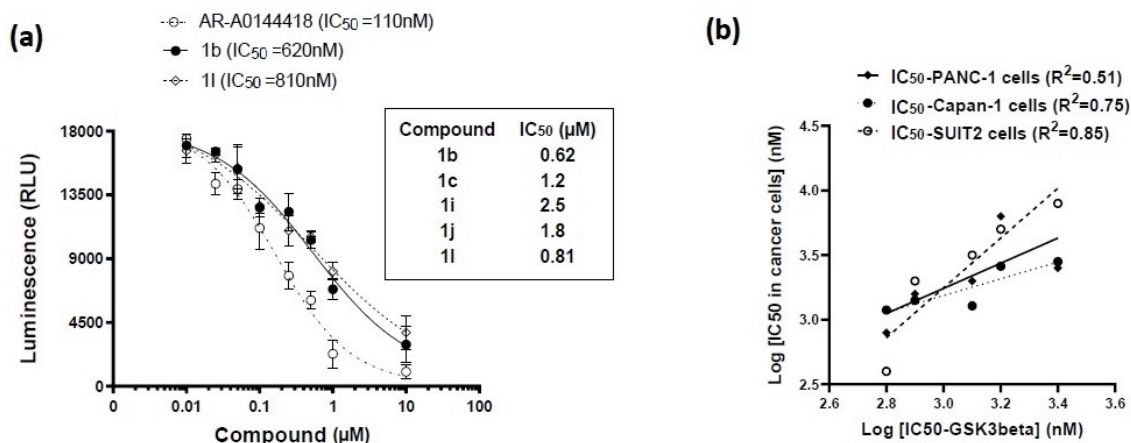


**Figure 10.** Effects of most active compounds **1b**, **1c**, **1i**, **1j** and **1I** on the *in vitro* GSK-3 $\beta$  kinase activity. (a) Determination of  $IC_{50}$  values of inhibitors using ADP-Glo™ assay. (b) Linear regression analyses to determine relationships between concentration achieving a 50% inhibition ( $IC_{50}$ ) of PDAC cell growth and half-maximal inhibitory concentration ( $IC_{50}$ ) in inhibiting the GSK-3 $\beta$  kinase activity.

lower potency ( $IC_{50}$  values in the range of 1.2–2.5  $\mu\text{M}$ ). In order to verify the accuracy of this method, AR-A0144418, a specific GSK-3 $\beta$  inhibitor, was used as positive control and its  $IC_{50}$  value was 0.11  $\mu\text{M}$ , in agreement with previous data from literature (0.104  $\mu\text{M}$ ).<sup>[39]</sup> These results indicate that our novel oxadiazole compounds are direct GSK-3 $\beta$  inhibitors *in vitro*. Despite the low number of data points, the anti-GSK3 $\beta$  activity seems to correlate with the  $IC_{50}$  values obtained in the antiproliferative assays, as reported in Figure 10b, with  $R^2$  values ranging from 0.51 to 0.85 and  $P$  values  $< 0.05$  at the Spearman analyses. A potential binding mode for the most active compounds **1b** and **1c** within the ATP binding site of GSK-3 $\beta$  is depicted in Figure 11. Both compounds were docked in the ATP binding site of GSK3 $\beta$  (PDB 1UV5)<sup>[40]</sup> showing similar interactions to the co-crystallized ligand 6-bromindirubin, a known potent and selective bis-indolyl inhibitor of the enzyme. Compounds **1b** and **11** are located into the same narrow hydrophobic pocket of the co-crystallized ligand, establishing a hydrogen bond through their indole nitrogen with the peptide carbonyl oxygen of Val135 residue. Moreover, their carbonyl group accepts a hydrogen bond from a water molecule interacting with Lys85, a residue that has been successfully targeted by carbonyl groups of potent inhibitors by direct or water-mediated interactions.<sup>[41,42]</sup>

### 3. Conclusion

A new series of sixteen topsentin analogues, characterized by a central 1,2,4-oxadiazole ring, was efficiently synthesized. Five of these new topsentin derivatives exhibited good antiproliferative activity against a panel of PDAC cells, namely SUIT-2, Capan-1 and Panc-1, with  $EC_{50}$  values ranging from micromolar to sub-micromolar level. A particular efficacy was observed for the compound **1b** against all PDAC preclinical models, showing  $EC_{50}$  values in the range of 0.40–1.19  $\mu\text{M}$ . The mechanism of the

anti-proliferative effect of these derivatives was pro-apoptotic, being associated with externalization of plasma membrane phosphatidylserine, a reliable marker of cell apoptosis. Through wound-healing assays we found remarkably reduction of cell migration in the metastatic Capan-1 PDAC preclinical model when treated with the most promising compound **1b**. These effects might be explained by interesting influence of the new topsentin analogues treatment on EMT determinants such as SNAIL-2 and metalloproteinase-9. Moreover, PathScan intracellular signaling and ELISA assays in Panc-1 cells revealed a significant inhibition of GSK3 $\beta$  phosphorylation, suggesting this kinase as a potential downstream target of our novel compounds. This was further supported by data from *in vitro* assay for GSK3 $\beta$  activity and molecular modelling. Future studies should investigate the kinase profiling data of our compounds against a wide range of kinases.

## Experimental Section

### Chemistry

Analytical thin layer chromatography (TLC) was performed on silica gel 60 F254 plates (0.25 mm thickness) and the develop plates were examined under ultraviolet (UV) light. All melting points were taken on a Buchi-Tottoly capillary apparatus and were uncorrected. IR spectra were determined in bromoform with a Shimadzu FT / IR 8400S spectrophotometer and peaks were reported in wavenumber ( $\text{cm}^{-1}$ ).  $^1\text{H}$  and  $^{13}\text{C}$  NMR spectra were measured at 200 and 50 MHz, respectively, on  $[\text{D}_6]$ DMSO solution, using a Bruker Avance II series 200 MHz spectrometer. Chromatography column was performed with MERK silica gel 230–400 mesh ASTM or FLASH40i Biotage chromatography or with Buchi Sepacore chromatography module (prepacked cartridge reference). Elementary analyses (C, H, N) were within  $\pm 0.4\%$  of the theoretical values and were performed with a VARIO EL III elemental analyzer (Elementar, Langensfeld, Germany). The HRMS have been obtained on a Thermo Q-Exactive system.

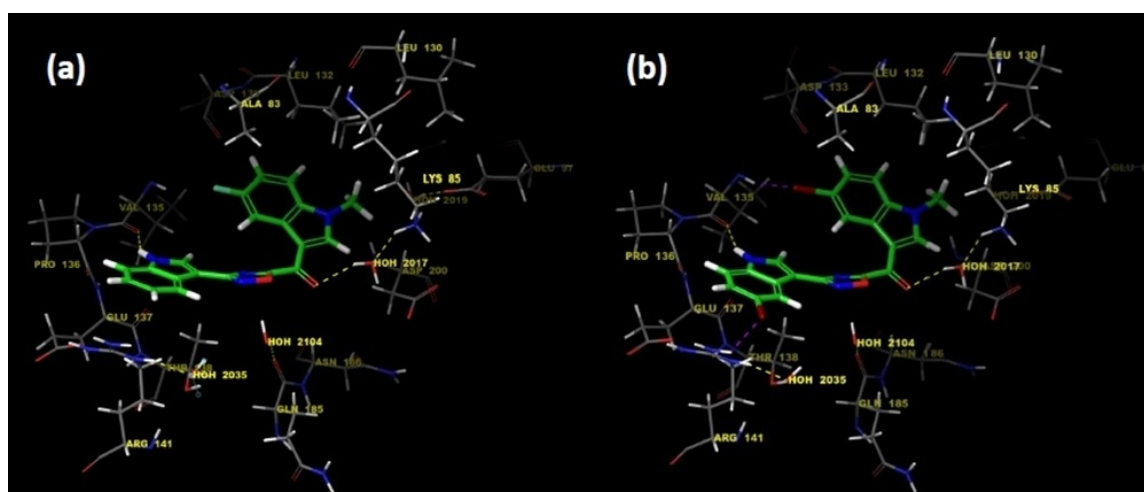


**Figure 11.** Proposed binding mode of compounds **1b** (a) and **11** (b) with GSK3 $\beta$  (PDB ID: 1UV5). H-bonds between the indole nitrogen of our compounds with the peptide carbonyl oxygen of Val135 residue, as well as the water-mediated interaction between the carbonyl group adjacent to oxadiazole ring and the Lys85 residue are shown with yellow dashed lines.

### General procedure for the synthesis of *N*-hydroxy-1*H*-indole-3-carboxamides (2a-d)

To a solution of the appropriate indole carbonitrile **4a-d** (2.88 mmol) in anhydrous ethanol (50 mL), *N,N*-diisopropylethylamine (DIPEA) (1.08 mL) and hydroxylamine hydrochloride (NH<sub>2</sub>OH·HCl) (530 mg, 7.63 mmol) were added in portions. The reaction mixture was heated to vigorous reflux for 4 hours. The solvent was removed under reduced pressure and the residue was treated with a saturated aqueous solution of sodium hydrogen carbonate (NaHCO<sub>3</sub>) (10 mL) and then extracted with ethyl acetate (3 × 20 mL), dried (Na<sub>2</sub>SO<sub>4</sub>), filtered and concentrated under vacuum. The product was purified by column chromatography using dichloromethane/ethyl acetate (DCM/EtOAc) or EtOAc as eluent.

**5-Bromo-*N'*-hydroxy-1*H*-indole-3-carboxamide (2a).** Eluent: DCM/EtOAc 75:25 (v/v); *R*<sub>f</sub> = 0.42 (EtOAc); white solid; yield: 85%; mp: 167.6–168.6 °C; <sup>1</sup>H NMR (200 MHz, [D<sub>6</sub>]DMSO) δ: 5.70 (s, 2H, NH<sub>2</sub>), 7.22 (dd, *J* = 8.6, 2.6 Hz, 1H, H-6), 7.36 (d, *J* = 8.6 Hz, 1H, H-7), 7.84 (d, *J* = 2.6 Hz, 1H, H-4), 8.27 (d, *J* = 1.9 Hz, 1H, H-2), 9.34 (s, 1H, OH), 11.47 (s, 1H, NH); <sup>13</sup>C NMR (50 MHz, [D<sub>6</sub>]DMSO) δ: 108.6 (s), 112.0 (s), 113.4 (d), 123.9 (d), 124.3 (d), 126.0 (d), 126.2 (s), 135.0 (s), 148.8 (s); IR (KBr): ν̄ = 3476 (OH), 3382 (NH<sub>2</sub>), 3310 (NH), 1653 cm<sup>-1</sup> (C=N); elemental analysis calcd (%) for C<sub>9</sub>H<sub>8</sub>BrN<sub>3</sub>O (MW: 254.08): C, 42.54; H, 3.17; N, 16.54; found: C, 42.70; H, 3.38; N, 16.32.

**5-Fluoro-*N'*-hydroxy-1*H*-indole-3-carboxamide (2b).** Eluent: EtOAc; *R*<sub>f</sub> = 0.38 (EtOAc); white solid; yield: 78%; mp: 142.7–143.7 °C; <sup>1</sup>H NMR (200 MHz, [D<sub>6</sub>]DMSO) δ: 5.64 (s, 2H, NH<sub>2</sub>), 6.96 (td, *J* = 9.1, 9.1, 2.7 Hz, 1H, H-6), 7.37 (dd, *J* = 9.1, 4.7 Hz, 1H, H-7), 7.73–7.86 (m, 2H, H-4 and H-2), 9.25 (s, 1H, OH), 11.36 (s, 1H, NH); <sup>13</sup>C NMR (50 MHz, [D<sub>6</sub>]DMSO) δ: 106.5 (d, *J*<sub>C4-F</sub> = 24.4 Hz), 109.1 (d, *J*<sub>C7a-F</sub> = 4.7 Hz), 109.7 (d, *J*<sub>C6-F</sub> = 26.1 Hz), 112.4 (d, *J*<sub>C7-F</sub> = 9.6 Hz), 124.7 (d, *J*<sub>C3a-F</sub> = 11.0 Hz), 126.4 (d), 133.0 (s), 149.1 (s), 157.1 (d, *J*<sub>C5-F</sub> = 231.9 Hz); IR (KBr): ν̄ = 3467 (OH), 3359 (NH<sub>2</sub>), 3200 (NH), 1630 cm<sup>-1</sup> (C=N); elemental analysis calcd (%) for C<sub>9</sub>H<sub>8</sub>FN<sub>3</sub>O (MW: 193.18): C, 55.96; H, 4.17; N, 21.75; found: C, 56.02; H, 4.38; N, 21.52.

***N'*-Hydroxy-1*H*-indole-3-carboxamide (2c).** Eluent: DCM/EtOAc 55:45 (v/v); *R*<sub>f</sub> = 0.33 (EtOAc); white solid; yield: 75%; mp: 147–148 °C; spectroscopic data in accordance with those reported in literature.<sup>[43]</sup>

**5-Methoxy-*N'*-hydroxy-1*H*-indole-3-carboxamide (2d).** Eluent: EtOAc; *R*<sub>f</sub> = 0.44 (EtOAc); white solid; yield: 80%; mp: 113.2–114.2 °C; <sup>1</sup>H NMR (200 MHz, [D<sub>6</sub>]DMSO) δ: 3.74 (s, 3H, OCH<sub>3</sub>), 5.59 (s, 2H, NH<sub>2</sub>), 6.75 (dd, *J* = 8.8, 2.5 Hz, 1H, H-6), 7.27 (d, *J* = 8.8 Hz, 1H, H-7), 7.58 (d, *J* = 2.5 Hz, 1H, H-4), 7.73 (s, 1H, H-2), 9.23 (s, 1H, OH), 11.11 (s, 1H, NH); <sup>13</sup>C NMR (50 MHz, [D<sub>6</sub>]DMSO) δ: 55.2 (q), 103.5 (d), 108.7 (s), 111.8 (d), 112.0 (d), 124.9 (s), 125.1 (d), 131.4 (s), 149.6 (s), 153.6 (s); IR (KBr): ν̄ = 3467 (OH), 3364 (NH<sub>2</sub>), 3279 (NH), 1634 cm<sup>-1</sup> (C=N); elemental analysis calcd (%) for C<sub>10</sub>H<sub>11</sub>N<sub>3</sub>O<sub>2</sub> (MW: 205.21): C, 58.53; H, 5.40; N, 20.48; found: C, 58.84; H, 5.21; N, 20.22.

### General procedure for the synthesis of (1-methyl-1*H*-indol-3-yl)-oxo-acetyl chlorides (7a–d)

To a solution of the opportune methyl-indole of the type **6** (10 mmol) in anhydrous diethyl ether (20 mL), oxalyl chloride (11.16 mmol, 0.95 mL) was added dropwise at 0 °C. The reaction mixture was left to stir at 0 °C for 3 hours and then brought to room temperature for 1 hour. The resulting solid product was collected by vacuum filtration and recrystallized from diethyl ether.

**(5-Bromo-1-methyl-1*H*-indol-3-yl)-oxo-acetyl chloride (7a).** *R*<sub>f</sub> = 0.68 (CH<sub>2</sub>Cl<sub>2</sub>/MeOH 6:4); yellow solid; yield: 91%; mp: 134.4–135.4 °C; <sup>1</sup>H NMR (200 MHz, [D<sub>6</sub>]DMSO) δ: 3.92 (s, 3H, CH<sub>3</sub>), 7.50 (dd, *J* = 8.7, 1.9 Hz, 1H, H-6), 7.61 (d, *J* = 8.7 Hz, 1H, H-7), 8.31 (d, *J* = 1.9 Hz, 1H,

H-4) 8.55 (s, 1H, H-2); <sup>13</sup>C NMR (50 MHz, [D<sub>6</sub>]DMSO) δ: 33.6 (q), 110.6 (s), 113.4 (d), 115.9 (s), 123.3 (d), 126.2 (d), 127.7 (s), 136.2 (s), 142.2 (d), 164.6 (s), 179.9 (s); IR (KBr): ν̄ = 1772 (CO), 1613 cm<sup>-1</sup> (CO); elemental analysis calcd (%) for C<sub>11</sub>H<sub>7</sub>BrClNO<sub>2</sub> (MW: 300.54): C, 43.96; H, 2.35; N, 4.66; found: C, 44.14; H, 2.29; N, 4.78.

**(5-Fluoro-1-methyl-1*H*-indol-3-yl)-oxo-acetyl chloride (7b).** *R*<sub>f</sub> = 0.75 (CH<sub>2</sub>Cl<sub>2</sub>/MeOH 6:4); yellow solid; yield: 96%; mp: 148.6–149.6 °C; <sup>1</sup>H NMR (200 MHz, [D<sub>6</sub>]DMSO) δ: 3.93 (s, 3H, CH<sub>3</sub>), 7.22 (td, *J* = 9.6, 9.2, 2.6 Hz, 1H, H-6), 7.64 (dd, *J* = 9.2, 4.4 Hz, 1H, H-7), 7.86 (dd, *J* = 9.6, 2.6 Hz, 1H, H-4), 8.55 (s, 1H, H-2); <sup>13</sup>C NMR (50 MHz, [D<sub>6</sub>]DMSO) δ: 33.7 (q), 106.2 (d, *J*<sub>C4-F</sub> = 24.8 Hz), 111.1 (d, *J*<sub>C7a-F</sub> = 4.4 Hz), 111.7 (d, *J*<sub>C6-F</sub> = 25.7 Hz), 112.7 (d, *J*<sub>C7-F</sub> = 9.8 Hz), 126.7 (d, *J*<sub>C3a-F</sub> = 11.2 Hz), 134.0 (s), 142.4 (d), 159.3 (d, *J*<sub>C5-F</sub> = 234.3 Hz), 166.4 (s), 181.2 (s); IR (KBr): ν̄ = 1743 (CO), 1642 cm<sup>-1</sup> (CO); elemental analysis calcd (%) for C<sub>11</sub>H<sub>7</sub>ClFNO<sub>2</sub> (MW: 239.63): C, 55.13; H, 2.94; N, 5.85; found: C, 54.98; H, 3.01; N, 5.69.

**(1-Methyl-1*H*-indol-3-yl)-oxo-acetyl chloride (7c).** *R*<sub>f</sub> = 0.66 (CH<sub>2</sub>Cl<sub>2</sub>/MeOH 6:4); yellow solid; yield: 89%; mp: 156.4–157.4 °C; <sup>1</sup>H NMR (200 MHz, [D<sub>6</sub>]DMSO) δ: 3.93 (s, 3H, CH<sub>3</sub>), 7.28–7.41 (m, 2H, H-5 and H-6), 7.59–7.64 (m, 1H, H-7), 8.18–8.23 (m, 1H, H-4), 8.50 (s, 1H, H-2); <sup>13</sup>C NMR (50 MHz, [D<sub>6</sub>]DMSO) δ: 33.4 (q), 111.1 (s), 111.2 (d), 121.2 (d), 123.1 (d), 123.7 (d), 126.0 (s), 137.35 (s), 141.3 (d), 165.1 (s), 180.0 (s); IR (KBr): ν̄ = 1735 (CO); 1604 cm<sup>-1</sup> (CO); elemental analysis calcd (%) for C<sub>11</sub>H<sub>8</sub>ClNO<sub>2</sub> (MW: 221.64): C, 59.61; H, 3.64; N, 6.32; found: C, 59.69; H, 3.70; N, 6.18.

**(5-Methoxy-1-methyl-1*H*-indol-3-yl)-oxo-acetyl chloride (7d).** *R*<sub>f</sub> = 0.60 (CH<sub>2</sub>Cl<sub>2</sub>/MeOH 6:4); orange solid; yield: 90%; mp: 132.2–133.2 °C; <sup>1</sup>H NMR (200 MHz, [D<sub>6</sub>]DMSO) δ: 3.82 (s, 3H, CH<sub>3</sub>), 3.89 (s, 3H, OCH<sub>3</sub>), 6.98 (dd, *J* = 8.9, 2.5 Hz, 1H, H-6), 7.52 (d, *J* = 8.9 Hz, 1H, H-7), 7.70 (d, *J* = 2.5 Hz, 1H, H-4), 8.42 (s, 1H, H-2); <sup>13</sup>C NMR (50 MHz, [D<sub>6</sub>]DMSO) δ: 33.5 (q), 55.3 (q), 103.2 (d), 110.9 (s), 112.0 (d), 113.1 (d), 127.0 (s), 132.2 (s), 141.0 (d), 156.4 (s), 165.3 (s), 180.0 (s); IR (KBr): ν̄ = 1779 (CO); 1625 cm<sup>-1</sup> (CO); elemental analysis calcd (%) for C<sub>12</sub>H<sub>10</sub>ClNO<sub>3</sub> (MW: 251.67): C, 57.27; H, 4.01; N, 5.57%; found: C, 57.19; H, 4.12; N, 5.37.

### General procedure for the synthesis of (1-methyl-1*H*-indol-3-yl)-oxo-acetic acids (3a–d)

To a solution of the suitable acyl chloride of the type **7** (10 mmol) in anhydrous tetrahydrofuran (THF) (20 mL), a solution of sodium hydroxide (NaOH) 2 M (15 mL) was added dropwise, until complete alkalization, reaching a pH of 14. The reaction mixture was stirred at room temperature overnight. A solution of hydrochloric acid (HCl) 6 M (10 mL) was added up to pH = 1. The resulting solid precipitate was collected by vacuum filtration, washed with water and dried under vacuum for 24 hours and purified by column chromatography using ethyl acetate as eluent to give desired oxo-acetic acids **3a-d**.

**(5-Bromo-1-methyl-1*H*-indol-3-yl)-oxo-acetic acid (3a).** *R*<sub>f</sub> = 0.20 (CH<sub>2</sub>Cl<sub>2</sub>/MeOH 8:2); yellow solid; yield: 87%; mp: 256.6 °C; <sup>1</sup>H NMR (200 MHz, [D<sub>6</sub>]DMSO) δ: 3.93 (s, 3H, CH<sub>3</sub>), 7.50 (dd, *J* = 8.7, 1.5 Hz, 1H, H-6), 7.62 (d, *J* = 8.7 Hz, 1H, H-7), 8.31 (d, *J* = 1.5 Hz, 1H, H-4), 8.55 (s, 1H, H-2), 14.03 (s, 1H, OH); <sup>13</sup>C NMR (50 MHz, [D<sub>6</sub>]DMSO) δ: 33.6 (q), 110.6 (s), 113.4 (d), 116.0 (s), 123.3 (d), 126.2 (d), 127.7 (s), 136.2 (s), 142.2 (d), 164.7 (s), 180.0 (s); IR (KBr): ν̄ = 3273 (OH), 1760 (CO), 1628 cm<sup>-1</sup> (CO); elemental analysis calcd (%) for C<sub>11</sub>H<sub>8</sub>BrNO<sub>3</sub> (MW: 282.09): C, 46.84; H, 2.86; N, 4.97; found: C, 46.54; H, 2.98; N, 5.04%.

**(5-Fluoro-1-methyl-1*H*-indol-3-yl)-oxo-acetic acid (3b).** *R*<sub>f</sub> = 0.16 (CH<sub>2</sub>Cl<sub>2</sub>/MeOH 8:2); yellow solid; yield: 95%; mp: 194.5 °C; <sup>1</sup>H NMR (200 MHz, [D<sub>6</sub>]DMSO) δ: 3.93 (s, 3H, CH<sub>3</sub>), 7.23 (td, *J* = 9.2, 9.1, 2.6 Hz, 1H, H-6), 7.66 (dd, *J* = 9.1, 4.5 Hz, 1H, H-7), 7.86 (dd, *J* = 9.2, 2.6 Hz,

1H, H-4), 8.56 (s, 1H, H-2), 13.94 (s, 1H, OH);  $^{13}\text{C}$  NMR (50 MHz,  $[\text{D}_6]\text{DMSO}$ )  $\delta$ : 33.7 (q), 106.2 (d,  $J_{\text{C}_4\text{-F}} = 24.8$  Hz), 111.1 (d,  $J_{\text{C}_7\text{a-F}} = 4.4$  Hz), 111.7 (d,  $J_{\text{C}_6\text{-F}} = 25.7$  Hz), 112.8 (d,  $J_{\text{C}_7\text{-F}} = 9.8$  Hz), 126.8 (d,  $J_{\text{C}_3\text{a-F}} = 11.2$  Hz), 134.0 (s), 142.4 (d), 159.3 (d,  $J_{\text{C}_5\text{-F}} = 234.3$  Hz), 164.8 (s), 179.9 (s); IR (KBr):  $\nu = 3216$  (OH), 1760 (CO), 1623  $\text{cm}^{-1}$  (CO); elemental analysis calcd (%) for  $\text{C}_{11}\text{H}_8\text{FNO}_3$  (MW: 221.18): C, 59.73; H, 3.65; N, 6.33; found: C, 59.84; H, 3.71; N, 6.83.

(1-Methyl-1H-indol-3-yl)-oxo-acetic acid (**3c**).  $R_f = 0.24$  ( $\text{CH}_2\text{Cl}_2/\text{MeOH}$  8:2); yellow solid; yield: 78%; mp: 150.6 °C;  $^1\text{H}$  NMR (200 MHz,  $[\text{D}_6]\text{DMSO}$ )  $\delta$ : 3.93 (s, 3H,  $\text{CH}_3$ ), 7.28–7.41 (m, 2H, H-5 and H-6), 7.62 (m, 1H, H-7), 8.20 (m, 1H, H-4), 8.49 (s, 1H, H-2), 13.88 (s, 1H, OH);  $^{13}\text{C}$  NMR (50 MHz,  $[\text{D}_6]\text{DMSO}$ )  $\delta$ : 33.4 (q), 111.1 (s), 111.2 (d), 121.2 (d), 123.1 (d), 123.7 (d), 126.0 (s), 137.3 (s), 141.3 (d), 165.2 (s), 180.2 (s); IR (KBr):  $\nu = 3261$  (OH), 1748 (CO), 1623  $\text{cm}^{-1}$  (CO); elemental analysis calcd (%) for  $\text{C}_{11}\text{H}_9\text{NO}_3$  (MW: 203.19): C, 65.02; H, 4.46; N, 6.89; Found: C, 65.18; H, 4.36; N, 6.99.

(5-Methoxy-1-methyl-1H-indol-3-yl)-oxo-acetic acid (**3d**).  $R_f = 0.22$  ( $\text{CH}_2\text{Cl}_2/\text{MeOH}$  8:2); yellow solid; yield: 86%; mp: 196.2 °C;  $^1\text{H}$  NMR (200 MHz,  $[\text{D}_6]\text{DMSO}$ )  $\delta$ : 3.82 (s, 3H,  $\text{CH}_3$ ), 3.89 (s, 3H,  $\text{OCH}_3$ ), 6.98 (dd,  $J = 8.9, 2.5$  Hz, 1H, H-6), 7.52 (d,  $J = 8.9$  Hz, 1H, H-7), 7.7 (d,  $J = 2.5$  Hz, 1H, H-4), 8.41 (s, 1H, H-2), 13.89 (s, 1H, OH);  $^{13}\text{C}$  NMR (50 MHz,  $[\text{D}_6]\text{DMSO}$ )  $\delta$ : 33.5 (q), 55.3 (q), 103.2 (d), 110.9 (s), 112.0 (d), 113.1 (d), 127.0 (s), 132.2 (s), 141.0 (d), 156.4 (s), 165.3 (s), 180.0 (s); IR (KBr):  $\nu = 3216$  (OH), 1765 (CO), 1628  $\text{cm}^{-1}$  (CO); elemental analysis calcd (%) for  $\text{C}_{12}\text{H}_{11}\text{NO}_4$  (MW: 233.22): C, 61.80; H, 4.75; N, 6.01; found: C, 61.60; H, 4.55; N, 6.21.

#### General procedure for the synthesis of [3-(1H-indol-3-yl)-1,2,4-oxadiazol-5-yl](1-methyl-1H-indol-3-yl) methanones (**1a-p**)

To a solution of the proper (1-methyl-1H-indol-3-yl)-oxo-acetic acid **3a-d** (1.42 mmol) and 1-hydroxybenzotriazole hydrate (HOBT) (230 mg, 1.7 mmol) in anhydrous dimethylformamide (DMF) (2 mL) at 0 °C, *N*-ethyl-*N'*-(3-dimethylaminopropyl)carbodiimide hydrochloride (EDC-HCl) (326 mg, 1.7 mmol) was added in portions. After 15 min, a DMF (1 mL) solution of triethylamine ( $\text{Et}_3\text{N}$ ) (0.2 mL, 1.42 mmol) and appropriate carboxamide **2a-d** (0.71 mmol) was added dropwise at 0 °C. The reaction mixture was stirred at 0 °C for 15 minutes. After bringing the reaction mixture to room temperature, it was heated at 100 °C for 15 minutes. After cooling, the mixture was poured into water and ice; the obtained precipitate was filtered off and dried under high vacuum. The crude was purified on flash chromatography, using dichloromethane as eluent, to obtain the desired products **1a-p**.

(5-Bromo-1-methyl-1H-indol-3-yl)[3-(1H-indol-3-yl)-1,2,4-oxadiazol-5-yl]methanone (**1a**).  $R_f = 0.78$  ( $\text{CH}_2\text{Cl}_2/\text{EtOAc}$  7:3); yellow solid; yield: 45%; mp: 255 °C (dec.);  $^1\text{H}$  NMR (200 MHz,  $[\text{D}_6]\text{DMSO}$ )  $\delta$ : 4.04 (s, 3H,  $\text{CH}_3$ ), 7.22–7.32 (m, 2H, H-5' and H-6'), 7.54–7.72 (m, 3H, H-6, H-7' and H-7), 8.07–8.11 (m, 1H, H-4'), 8.43–8.46 (m, 2H, H-4 and H-2'), 9.16 (s, 1H, H-2), 12.07 (s, 1H, NH);  $^{13}\text{C}$  NMR (50 MHz,  $[\text{D}_6]\text{DMSO}$ )  $\delta$ : 33.9 (q), 101.9 (s), 112.0 (s), 112.4 (d), 113.7 (d), 116.4 (s), 120.5 (d), 121.1 (d), 122.7 (d), 123.6 (d), 124.2 (s), 126.6 (d), 128.1 (s), 129.9 (d), 136.4 (s), 136.8 (s), 143.2 (d), 165.4 (s), 169.2 (s), 170.4 (s); IR (KBr):  $\nu = 3280$  (NH), 1623  $\text{cm}^{-1}$  (CO); elemental analysis calcd (%) for  $\text{C}_{20}\text{H}_{13}\text{BrN}_4\text{O}_2$  (MW: 421.25): C, 57.02; H, 3.11; N, 13.30; found: C, 57.10; H, 3.21; N, 13.24.

(5-Fluoro-1-methyl-1H-indol-3-yl)[3-(1H-indol-3-yl)-1,2,4-oxadiazol-5-yl]methanone (**1b**).  $R_f = 0.77$  ( $\text{CH}_2\text{Cl}_2/\text{EtOAc}$  7:3); yellow solid; yield: 46%; mp: 248 °C (dec.);  $^1\text{H}$  NMR (200 MHz,  $[\text{D}_6]\text{DMSO}$ )  $\delta$ : 4.05 (s, 3H,  $\text{CH}_3$ ), 7.25–7.32 (m, 3H, H-5', H-6' and H-6), 7.55–7.59 (m, 1H, H-7'), 7.74 (dd,  $J = 8.9, 2.4$  Hz, 1H, H-7), 7.98–8.12 (m, 2H, H-4' and H-4), 8.43 (d,  $J = 2.8$  Hz, 1H, H-2'), 9.17 (s, 1H, H-2), 12.06 (s, 1H, NH);  $^{13}\text{C}$

NMR (50 MHz,  $[\text{D}_6]\text{DMSO}$ )  $\delta$ : 34.0 (q), 99.5 (d), 101.9 (s), 106.6 (d,  $J_{\text{C}_4\text{-F}} = 25.4$  Hz), 112.1 (d,  $J_{\text{C}_6\text{-F}} = 29.2$  Hz), 112.6 (d,  $J_{\text{C}_7\text{a-F}} = 4.0$  Hz), 113.1 (d,  $J_{\text{C}_7\text{-F}} = 9.7$  Hz), 120.5 (d), 121.1 (d), 122.7 (d), 124.2 (s), 127.2 (d,  $J_{\text{C}_3\text{a-F}} = 10.9$  Hz), 129.9 (d), 134.2 (s), 136.8 (s), 143.5 (d), 159.6 (d,  $J_{\text{C}_5\text{-F}} = 237.3$  Hz), 165.4 (s), 169.3 (s), 170.3 (s); IR (KBr):  $\nu = 3281$  (NH), 1617  $\text{cm}^{-1}$  (CO); elemental analysis calcd (%) for  $\text{C}_{20}\text{H}_{13}\text{FN}_4\text{O}_2$  (MW: 360.34): C, 66.66; H, 3.64; N, 15.55; found: C, 66.78; H, 3.51; N, 15.34; HRMS:  $m/z = 361.11$  [ $\text{M} + \text{H}$ ] $^+$ ;  $t_R = 3.57$  min (> 98% purity).

[3-(1H-Indol-3-yl)-1,2,4-oxadiazol-5-yl](1-methyl-1H-indol-3-yl)methanone (**1c**).  $R_f = 0.83$  ( $\text{CH}_2\text{Cl}_2/\text{EtOAc}$  7:3); yellow solid; yield: 50%; mp: 230 °C (dec.);  $^1\text{H}$  NMR (200 MHz,  $[\text{D}_6]\text{DMSO}$ )  $\delta$ : 4.04 (s, 3H,  $\text{CH}_3$ ), 7.23–7.33 (m, 2H, H-5 and H-5'), 7.40–7.47 (m, 2H, H-6 and H-6'), 7.55–7.60 (m, 1H, H-7'), 7.68–7.72 (m, 1H, H-7), 8.07–8.13 (m, 1H, H-4'), 8.33–8.37 (m, 1H, H-4), 8.43 (d,  $J = 2.8$  Hz, 1H, H-2'), 9.13 (s, 1H, H-2), 12.07 (s, 1H, NH);  $^{13}\text{C}$  NMR (50 MHz,  $[\text{D}_6]\text{DMSO}$ )  $\delta$ : 33.7 (q), 102.0 (d), 111.4 (d), 112.4 (d), 112.7 (s), 120.5 (d), 121.1 (d), 121.5 (d), 122.7 (d), 123.6 (d), 124.1 (d), 124.2 (s), 126.4 (s), 129.8 (d), 136.8 (s), 137.5 (s), 142.5 (d), 165.3 (s), 169.6 (s), 170.4 (s); IR (KBr):  $\nu = 3393$  (NH), 1617  $\text{cm}^{-1}$  (CO); elemental analysis calcd (%) for  $\text{C}_{20}\text{H}_{14}\text{N}_4\text{O}_2$  (MW: 342.35): C, 70.17; H, 4.12; N, 16.37; found: C, 70.30; H, 4.30; N, 16.14; HRMS:  $m/z = 343.12$  [ $\text{M} + \text{H}$ ] $^+$ ;  $t_R = 3.52$  min (> 98% purity).

[3-(1H-Indol-3-yl)-1,2,4-oxadiazol-5-yl](5-methoxy-1-methyl-1H-indol-3-yl)methanone (**1d**).  $R_f = 0.78$  ( $\text{CH}_2\text{Cl}_2/\text{EtOAc}$  7:3); yellow solid; yield: 48%; mp: 258 °C (dec.);  $^1\text{H}$  NMR (200 MHz,  $[\text{D}_6]\text{DMSO}$ )  $\delta$ : 3.86 (s, 3H,  $\text{CH}_3$ ), 4.01 (s, 3H,  $\text{OCH}_3$ ), 7.04 (dd,  $J = 8.9, 2.4$  Hz, 1H, H-6'), 7.23–7.33 (m, 2H, H-5 and H-6), 7.55–7.62 (m, 2H, H-7' and H-7), 7.85 (d,  $J = 2.4$  Hz, 1H, H-4'), 8.08–8.13 (m, 1H, H-4), 8.42 (d,  $J = 2.4$  Hz, 1H, H-2'), 9.04 (s, 1H, H-2), 12.05 (s, 1H, NH);  $^{13}\text{C}$  NMR (50 MHz,  $[\text{D}_6]\text{DMSO}$ )  $\delta$ : 33.9 (q), 55.4 (q), 102.0 (s), 103.5 (d), 112.4 (d), 113.4 (d), 120.5 (d), 121.1 (d), 122.7 (d), 124.2 (s), 127.4 (s), 129.6 (d), 129.8 (d), 132.4 (s), 133.5 (s), 136.8 (s), 142.2 (d), 156.8 (s), 165.3 (s), 169.6 (s), 170.2 (s); IR (KBr):  $\nu = 3228$  (NH), 1617  $\text{cm}^{-1}$  (CO); elemental analysis calcd (%) for  $\text{C}_{21}\text{H}_{16}\text{N}_4\text{O}_3$  (MW: 372.38): C, 67.73; H, 4.33; N, 15.05; found: C, 67.92; H, 4.12; N, 15.14.

(5-Fluoro-1-methyl-1H-indol-3-yl)[3-(5-methoxy-1H-indol-3-yl)-1,2,4-oxadiazol-5-yl]methanone (**1e**).  $R_f = 0.72$  ( $\text{CH}_2\text{Cl}_2/\text{EtOAc}$  7:3); Yellow solid; yield: 60%; mp: 262 °C (dec.);  $^1\text{H}$  NMR (200 MHz,  $[\text{D}_6]\text{DMSO}$ )  $\delta$ : 3.85 (s, 3H,  $\text{CH}_3$ ), 4.04 (s, 3H,  $\text{OCH}_3$ ), 6.92 (dd,  $J = 8.8, 2.4$  Hz, 1H, H-6'), 7.29 (td,  $J = 9.2, 9.2, 2.6$  Hz, 1H, H-6), 7.46 (d,  $J = 8.8$  Hz, 1H, H-7'), 7.56 (d,  $J = 2.4$  Hz, 1H, H-4'), 7.74 (dd,  $J = 9.2, 4.4$  Hz, 1H, H-7), 8.01 (dd,  $J = 9.6, 2.6$  Hz, 1H, H-4), 8.36 (d,  $J = 2.9$  Hz, 1H, H-2'), 9.17 (s, 1H, H-2), 11.94 (s, 1H, NH);  $^{13}\text{C}$  NMR (50 MHz,  $[\text{D}_6]\text{DMSO}$ )  $\delta$ : 34.0 (q), 55.2 (q), 101.7 (s), 102.0 (d), 106.6 (d,  $J_{\text{C}_4\text{-F}} = 25.5$  Hz), 112.1 (d,  $J_{\text{C}_6\text{-F}} = 25.7$  Hz), 112.6 (d,  $J_{\text{C}_7\text{a-F}} = 4.8$  Hz), 112.8 (d), 113.1 (d,  $J_{\text{C}_7\text{-F}} = 10.2$  Hz), 113.2 (d), 124.8 (s), 127.2 (d,  $J_{\text{C}_3\text{a-F}} = 11.4$  Hz), 130.0 (d), 131.7 (s), 134.2 (s), 143.4 (d), 154.8 (s), 159.6 (d,  $J_{\text{C}_5\text{-F}} = 237.0$  Hz), 165.4 (s), 169.3 (s), 170.3 (s); IR (KBr):  $\nu = 3267$  (NH), 1623  $\text{cm}^{-1}$  (CO); elemental analysis calcd (%) for  $\text{C}_{21}\text{H}_{15}\text{FN}_4\text{O}_3$  (MW: 390.37): C, 64.61; H, 3.87; N, 14.35; found: C, 64.70; H, 3.61; N, 14.24.

[3-(5-Methoxy-1H-indol-3-yl)-1,2,4-oxadiazol-5-yl](5-methoxy-1-methyl-1H-indol-3-yl)methanone (**1f**).  $R_f = 0.74$  ( $\text{CH}_2\text{Cl}_2/\text{EtOAc}$  7:3); yellow solid; yield: 62%; mp: 244 °C (dec.);  $^1\text{H}$  NMR (200 MHz,  $[\text{D}_6]\text{DMSO}$ )  $\delta$ : 3.86 (bs, 6H,  $\text{CH}_3$  and  $\text{OCH}_3$ ), 4.00 (s, 3H,  $\text{OCH}_3$ ), 6.92 (dd,  $J = 8.9, 2.3$  Hz, 1H, H-6'), 7.03 (dd,  $J = 8.9, 2.3$  Hz, 1H, H-6), 7.46 (d,  $J = 8.9$  Hz, 1H, H-7), 7.56–7.62 (m, 2H, H-7 and H-4), 7.85 (d,  $J = 2.3$  Hz, 1H, H-4), 8.34 (d,  $J = 2.7$  Hz, 1H, H-2'), 9.03 (s, 1H, H-2), 11.93 (s, 1H, NH);  $^{13}\text{C}$  NMR (50 MHz,  $[\text{D}_6]\text{DMSO}$ )  $\delta$ : 33.83 (q), 55.3 (q), 55.4 (q), 101.7 (s), 102.0 (d), 103.6 (d), 112.3 (d), 112.5 (s), 112.8 (d), 113.2 (d), 113.4 (d), 124.8 (s), 127.4 (s), 129.9 (d), 131.7 (s), 132.4 (s), 142.2 (d), 154.8 (s), 156.8 (s), 165.3 (s), 169.6 (s), 170.2 (s); IR (KBr):  $\nu = 3290$  (NH), 1627  $\text{cm}^{-1}$  (CO); elemental analysis calcd (%) for  $\text{C}_{22}\text{H}_{18}\text{N}_4\text{O}_4$  (MW: 402.40): C, 65.66; H, 4.51; N, 13.92; found: C, 65.76; H, 4.61; N, 14.04.

(5-Bromo-1-methyl-1H-indol-3-yl)[3-(5-methoxy-1H-indol-3-yl)-1,2,4-oxadiazol-5-yl]methanone (**1g**).  $R_f = 0.76$  ( $\text{CH}_2\text{Cl}_2/\text{EtOAc}$  7:3); yellow

solid; yield: 52%; mp: 274 °C (dec.); <sup>1</sup>H NMR (200 MHz, [D<sub>6</sub>]DMSO) δ: 3.85 (s, 3H, CH<sub>3</sub>), 4.03 (s, 3H, OCH<sub>3</sub>), 6.92 (dd, *J* = 8.9, 2.4 Hz, 1H, H-6'), 7.46 (d, *J* = 8.9 Hz, 1H, H-7'), 7.55–7.60 (m, 2H, H-6 and H-4'), 7.70 (d, *J* = 8.7 Hz, 1H, H-7), 8.35 (d, *J* = 2.8 Hz, 1H, H-2'), 8.46 (d, *J* = 1.6 Hz, 1H, H-4), 9.16 (s, 1H, H-2), 11.93 (s, 1H, NH); <sup>13</sup>C NMR (50 MHz, [D<sub>6</sub>]DMSO) δ: 33.9 (q), 55.2 (q), 101.7 (s), 102.0 (d), 112.0 (s), 112.8 (d), 113.2 (d), 113.6 (d), 116.4 (s), 123.6 (d), 124.8 (s), 126.6 (d), 128.1 (s), 130.0 (d), 131.7 (s), 136.3 (s), 143.2 (d), 154.8 (s), 165.4 (s), 169.2 (s), 170.3 (s); IR (KBr): ν<sup>-</sup> = 3312 (NH), 1623 cm<sup>-1</sup> (CO); elemental analysis calcd (%) for C<sub>21</sub>H<sub>15</sub>BrN<sub>4</sub>O<sub>3</sub> (MW: 451.27): C, 55.89; H, 3.35; N, 12.42; found: C, 56.02; H, 3.61; N, 12.08.

[3-(5-Methoxy-1H-indol-3-yl)-1,2,4-oxadiazol-5-yl](1-methyl-1H-indol-3-yl)methanone (**1h**). *R*<sub>f</sub> = 0.79 (CH<sub>2</sub>Cl<sub>2</sub>/EtOAc 7:3); yellow solid; yield: 56%; mp: 247 °C (dec.); <sup>1</sup>H NMR (200 MHz, [D<sub>6</sub>]DMSO) δ: 3.86 (s, 3H, CH<sub>3</sub>), 4.04 (s, 3H, OCH<sub>3</sub>), 6.92 (dd, *J* = 8.9, 2.3 Hz, 1H, H-6'), 7.36–7.49 (m, 3H, H-5, H-6 and H-7'), 7.56 (d, *J* = 2.3 Hz, 1H, H-4'), 7.67–7.71 (m, 1H, H-7), 8.33–8.37 (m, 2H, H-4 and H-2'), 9.12 (s, 1H, H-2), 11.94 (s, 1H, NH); <sup>13</sup>C NMR (50 MHz, [D<sub>6</sub>]DMSO) δ: 34.1 (q), 55.8 (q), 102.2 (s + d), 102.6 (s), 111.3 (s), 111.9 (d), 113.7 (d), 122.0 (d), 124.0 (d), 124.6 (d), 125.4 (s), 126.9 (d), 130.4 (d), 132.2 (s), 138.0 (s), 142.9 (d), 155.3 (s), 165.9 (s), 170.1 (s), 170.9 (s); IR (KBr): ν<sup>-</sup> = 3302 (NH), 1616 cm<sup>-1</sup> (CO); elemental analysis calcd (%) for C<sub>21</sub>H<sub>16</sub>N<sub>4</sub>O<sub>3</sub> (MW: 372.38): C, 67.73; H, 4.33; N, 15.05; found: C, 67.70; H, 4.51; N, 15.20.

[3-(5-Bromo-1H-indol-3-yl)-1,2,4-oxadiazol-5-yl](5-methoxy-1-methyl-1H-indol-3-yl)methanone (**1i**). *R*<sub>f</sub> = 0.69 (CH<sub>2</sub>Cl<sub>2</sub>/EtOAc 7:3); yellow solid; yield: 78%; mp: 258 °C (dec.); <sup>1</sup>H NMR (200 MHz, [D<sub>6</sub>]DMSO) δ: 3.85 (s, 3H, CH<sub>3</sub>), 4.00 (s, 3H, OCH<sub>3</sub>), 7.03 (dd, *J* = 8.9, 2.5 Hz, 1H, H-6), 7.41 (dd, *J* = 8.6, 1.9 Hz, 1H, H-6'), 7.53–7.61 (m, 2H, H-7 and H-7'), 7.83 (d, *J* = 2.5 Hz, 1H, H-4), 8.21 (d, *J* = 1.9 Hz, 1H, H-4'), 8.47 (d, *J* = 2.8 Hz, 1H, H-2'), 9.02 (s, 1H, H-2), 12.27 (s, 1H, NH); <sup>13</sup>C NMR (50 MHz, [D<sub>6</sub>]DMSO) δ: 33.9 (q), 55.4 (q), 101.6 (s), 103.5 (d), 112.4 (d), 112.5 (s), 113.4 (d), 113.6 (s), 114.5 (d), 122.6 (d), 125.3 (d), 125.9 (s), 127.4 (s), 131.1 (d), 132.3 (s), 135.6 (s), 142.2 (d), 156.8 (s), 164.9 (s), 169.8 (s), 170.0 (s); IR (KBr): ν<sup>-</sup> = 3302 (NH), 1610 cm<sup>-1</sup> (CO); elemental analysis calcd (%) for C<sub>21</sub>H<sub>15</sub>BrN<sub>4</sub>O<sub>3</sub> (MW: 451.27): C, 55.89; H, 3.35; N, 12.42; found: C, 55.70; H, 3.51; N, 12.24; HRMS: *m/z* = 451.04 [M + H]<sup>+</sup>; *t*<sub>R</sub> = 3.65 min (> 99% purity).

[3-(5-Bromo-1H-indol-3-yl)-1,2,4-oxadiazol-5-yl](1-methyl-1H-indol-3-yl)methanone (**1j**). *R*<sub>f</sub> = 0.75 (CH<sub>2</sub>Cl<sub>2</sub>/EtOAc 7:3); yellow solid; yield: 46%; mp: 271 °C (dec.); <sup>1</sup>H NMR (200 MHz, [D<sub>6</sub>]DMSO) δ: 4.04 (s, 3H, CH<sub>3</sub>), 7.36–7.47 (m, 3H, H-5, H-6 and H-6'), 7.56 (d, *J* = 8.6 Hz, 1H, H-7'), 7.67–7.72 (m, 1H, H-7), 8.22 (d, *J* = 1.8 Hz, 1H, H-4'), 8.32–8.37 (m, 1H, H-4), 8.48 (d, *J* = 2.8 Hz, 1H, H-2'), 9.11 (s, 1H, H-2), 12.27 (s, 1H, NH); <sup>13</sup>C NMR (50 MHz, [D<sub>6</sub>]DMSO) δ: 33.7 (q), 101.6 (s), 111.4 (d), 112.7 (s), 113.7 (s), 114.6 (d), 121.5 (d), 122.6 (d), 123.6 (d), 124.1 (d), 125.3 (d), 125.9 (s), 126.4 (s), 131.1 (d), 135.6 (s), 137.5 (s), 142.5 (d), 164.9 (s), 169.8 (s), 170.2 (s); IR (KBr): ν<sup>-</sup> = 3376 (NH), 1618 cm<sup>-1</sup> (CO); elemental analysis calcd (%) for C<sub>20</sub>H<sub>13</sub>BrN<sub>4</sub>O<sub>2</sub> (MW: 421.25): C, 57.02; H, 3.11; N, 13.30; found: C, 56.92; H, 3.02; N, 13.14; HRMS: *m/z* = 421.03 [M + H]<sup>+</sup>; *t*<sub>R</sub> = 3.68 min (> 99% purity).

[3-(5-Bromo-1H-indol-3-yl)-1,2,4-oxadiazol-5-yl](5-fluoro-1-methyl-1H-indol-3-yl)methanone (**1k**). *R*<sub>f</sub> = 0.70 (CH<sub>2</sub>Cl<sub>2</sub>/EtOAc 7:3); yellow solid; yield: 58%; mp: 277 °C (dec.); <sup>1</sup>H NMR (200 MHz, [D<sub>6</sub>]DMSO) δ: 4.04 (s, 3H, CH<sub>3</sub>), 7.29 (td, *J* = 9.2, 9.2, 2.6 Hz, 1H, H-6), 7.41 (dd, *J* = 8.7, 1.9 Hz, 1H, H-6'), 7.55 (d, *J* = 8.7 Hz, 1H, H-7'), 7.73 (dd, *J* = 9.2, 4.4 Hz, 1H, H-7), 8.00 (dd, *J* = 9.5, 2.6 Hz, 1H, H-4), 8.20 (d, *J* = 1.9 Hz, 1H, H-4'), 8.48 (d, *J* = 2.1 Hz, 1H, H-2'), 9.16 (s, 1H, H-2), 12.27 (s, 1H, NH); <sup>13</sup>C NMR (50 MHz, [D<sub>6</sub>]DMSO) δ: 34.0 (q), 101.54 (s), 106.6 (d, *J*<sub>C4-F</sub> = 24.9 Hz), 112.1 (d, *J*<sub>C6-F</sub> = 26.4 Hz), 112.5 (d, *J*<sub>C7a-F</sub> = 4.2 Hz), 113.1 (d, *J*<sub>C7-F</sub> = 10.2 Hz), 113.7 (s), 114.6 (d), 122.6 (d), 125.3 (d), 125.9 (s), 127.2 (d, *J*<sub>C3a-F</sub> = 11.3 Hz), 131.1 (d), 134.1 (s), 135.6 (s), 143.6 (d), 159.6 (d, *J*<sub>C5-F</sub> = 236.0 Hz), 164.9 (s), 169.5 (s), 170.1 (s); IR (KBr): ν<sup>-</sup> = 3267 (NH), 1615 cm<sup>-1</sup> (CO); elemental analysis calcd (%) for

C<sub>20</sub>H<sub>12</sub>BrFN<sub>4</sub>O<sub>2</sub> (MW: 439.24): C, 54.69; H, 2.75; N, 12.76; found: C, 54.55; H, 2.60; N, 13.00.

[3-(5-Bromo-1H-indol-3-yl)-1,2,4-oxadiazol-5-yl](5-bromo-1-methyl-1H-indol-3-yl)methanone (**1l**). *R*<sub>f</sub> = 0.66 (CH<sub>2</sub>Cl<sub>2</sub>/EtOAc 7:3); yellow solid; yield: 73%; mp: 294 °C (dec.); <sup>1</sup>H NMR (200 MHz, [D<sub>6</sub>]DMSO) δ: 4.04 (s, 3H, CH<sub>3</sub>), 7.42 (dd, *J* = 8.6, 1.8 Hz, 1H, H-6'), 7.54–7.60 (m, 2H, H-6 and H-7), 7.70 (d, *J* = 8.6 Hz, 1H, H-7'), 8.21 (d, *J* = 1.8 Hz, 1H, H-4'), 8.46 (d, *J* = 1.6 Hz, 1H, H-4), 8.49 (s, 1H, H-2'), 9.16 (s, 1H, H-2), 12.28 (s, 1H, NH); <sup>13</sup>C NMR (50 MHz, [D<sub>6</sub>]DMSO) δ: 33.9 (q), 101.5 (s), 112.0 (s), 113.7 (d), 114.5 (d), 116.4 (s), 122.6 (d), 123.5 (d), 125.3 (d), 125.9 (s), 126.6 (d), 128.1 (s), 131.2 (d), 135.6 (s), 136.3 (s), 143.2 (d), 158.7 (s), 164.9 (s), 169.4 (s), 170.1 (s); IR (KBr): ν<sup>-</sup> = 3341 (NH), 1617 cm<sup>-1</sup> (CO); elemental analysis calcd (%) for C<sub>20</sub>H<sub>12</sub>Br<sub>2</sub>N<sub>4</sub>O<sub>2</sub> (MW: 500.14): C, 48.03; H, 2.42; N, 11.20; found: C, 48.12; H, 2.60; N, 11.05; HRMS: *m/z* = 498.94 [M + H]<sup>+</sup>; *t*<sub>R</sub> = 3.84 min (> 99% purity).

[3-(5-Fluoro-1H-indol-3-yl)-1,2,4-oxadiazol-5-yl](1-methyl-1H-indol-3-yl)methanone (**1m**). *R*<sub>f</sub> = 0.71 (CH<sub>2</sub>Cl<sub>2</sub>/EtOAc 7:3); yellow solid; yield: 59%; mp: 261 °C (dec.); <sup>1</sup>H NMR (200 MHz, [D<sub>6</sub>]DMSO) δ: 4.04 (s, 3H, CH<sub>3</sub>), 7.15 (td, *J* = 9.4, 9.1, 2.4 Hz, 1H, H-6'), 7.39–7.43 (m, 2H, H-5 and H-6), 7.59 (dd, *J* = 9.1, 4.5 Hz, 1H, H-7'), 7.67–7.78 (m, 2H, H-7 and H-4'), 8.32–8.36 (m, 1H, H-4), 8.49 (s, 1H, H-2'), 9.11 (s, 1H, H-2), 12.18 (s, 1H, NH); <sup>13</sup>C NMR (50 MHz, [D<sub>6</sub>]DMSO) δ: 33.7 (q), 102.1 (d, *J*<sub>C7a-F</sub> = 4.5 Hz), 105.2 (d, *J*<sub>C4-F</sub> = 23.6 Hz), 111.0 (d, *J*<sub>C6-F</sub> = 26.0 Hz), 111.4 (d), 112.7 (s), 113.7 (d, *J*<sub>C7-F</sub> = 12.0 Hz), 121.5 (d), 123.6 (d), 124.1 (d), 124.6 (d, *J*<sub>C3a-F</sub> = 11.2 Hz), 126.4 (s), 131.5 (d), 133.5 (s), 137.5 (s), 142.5 (d), 158.0 (d, *J*<sub>C5-F</sub> = 234.6 Hz), 165.0 (s), 169.7 (s), 170.3 (s); IR (KBr): ν<sup>-</sup> = 3284 (NH), 1623 cm<sup>-1</sup> (CO); elemental analysis calcd (%) for C<sub>20</sub>H<sub>13</sub>FN<sub>4</sub>O<sub>2</sub> (MW: 360.34): C, 66.66; H, 3.64; N, 15.55; found: C, 66.70; H, 3.60; N, 15.22.

[3-(5-Fluoro-1H-indol-3-yl)-1,2,4-oxadiazol-5-yl](5-fluoro-1-methyl-1H-indol-3-yl)methanone (**1n**). *R*<sub>f</sub> = 0.65 (CH<sub>2</sub>Cl<sub>2</sub>/EtOAc 7:3); yellow solid; yield: 63%; mp: 265 °C (dec.); <sup>1</sup>H NMR (200 MHz, [D<sub>6</sub>]DMSO) δ: 4.03 (s, 3H, CH<sub>3</sub>), 7.15 (td, *J* = 9.2, 9.1, 2.6 Hz, 1H, H-6'), 7.30 (td, *J* = 9.2, 9.1, 2.6 Hz, 1H, H-6), 7.60 (dd, *J* = 9.1, 4.6 Hz, 1H, H-7'), 7.71–7.77 (m, 2H, H-7 and H-4'), 8.01 (dd, *J* = 9.6, 2.6 Hz, 1H, H-4), 8.50 (d, *J* = 2.9 Hz, 1H, H-2'), 9.16 (s, 1H, H-2), 12.19 (s, 1H, NH); <sup>13</sup>C NMR (50 MHz, [D<sub>6</sub>]DMSO) δ: 34.0 (q), 102.1 (d, *J*<sub>C7a-F</sub> = 4.3 Hz), 105.2 (d, *J*<sub>C4-F</sub> = 25.1 Hz), 106.6 (d, *J*<sub>C4-F</sub> = 24.9 Hz), 111.0 (d, *J*<sub>C6-F</sub> = 26.4 Hz), 112.1 (d, *J*<sub>C6-F</sub> = 25.7 Hz), 112.5 (d, *J*<sub>C7a-F</sub> = 4.2 Hz), 113.1 (d, *J*<sub>C7-F</sub> = 9.5 Hz), 113.7 (d, *J*<sub>C7-F</sub> = 9.7 Hz), 124.6 (d, *J*<sub>C3a-F</sub> = 11.2 Hz), 127.2 (d, *J*<sub>C3a-F</sub> = 11.1 Hz), 131.5 (d), 133.4 (s), 134.2 (s), 143.5 (d), 158.0 (d, *J*<sub>C5-F</sub> = 234.1 Hz), 159.6 (d, *J*<sub>C5-F</sub> = 235.3 Hz), 165.0 (s), 169.4 (s), 170.1 (s); IR (KBr): ν<sup>-</sup> = 3267 (NH), 1615 cm<sup>-1</sup> (CO); elemental analysis calcd (%) for C<sub>20</sub>H<sub>12</sub>F<sub>2</sub>N<sub>4</sub>O<sub>2</sub> (MW: 378.33): C, 63.49; H, 3.20; N, 14.81; found: C, 63.60; H, 3.32; N, 15.00.

[3-(5-Fluoro-1H-indol-3-yl)-1,2,4-oxadiazol-5-yl](5-methoxy-1-methyl-1H-indol-3-yl)methanone (**1o**). *R*<sub>f</sub> = 0.66 (CH<sub>2</sub>Cl<sub>2</sub>/EtOAc 7:3); yellow solid; yield: 62%; mp: 218 °C (dec.); <sup>1</sup>H NMR (200 MHz, [D<sub>6</sub>]DMSO) δ: 3.86 (s, 3H, CH<sub>3</sub>), 4.00 (s, 3H, OCH<sub>3</sub>), 7.04 (dd, *J* = 8.9, 2.5 Hz, 1H, H-6), 7.15 (td, *J* = 9.2, 9.1, 2.6 Hz, 1H, H-6'), 7.55–7.62 (m, 2H, H-7 and H-7'), 7.74 (dd, *J* = 9.7, 2.6 Hz, 1H, H-4'), 7.84 (d, *J* = 2.5 Hz, 1H, H-4), 8.48 (d, *J* = 2.7 Hz, 1H, H-2'), 9.03 (s, 1H, H-2), 12.18 (s, 1H, NH); <sup>13</sup>C NMR (50 MHz, [D<sub>6</sub>]DMSO) δ: 33.9 (q), 55.4 (q), 102.1 (d, *J*<sub>C7a-F</sub> = 4.5 Hz), 103.5 (d), 105.2 (d, *J*<sub>C4-F</sub> = 24.7 Hz), 111.0 (d, *J*<sub>C6-F</sub> = 26.1 Hz), 112.4 (d), 112.5 (s), 113.4 (d), 113.7 (d, *J*<sub>C7-F</sub> = 9.5 Hz), 124.6 (d, *J*<sub>C3a-F</sub> = 11.1 Hz), 127.4 (s), 131.5 (d), 132.3 (s), 133.4 (s), 142.2 (d), 156.8 (s), 158.0 (d, *J*<sub>C5-F</sub> = 234.4 Hz), 165.0 (s), 169.8 (s), 170.0 (s); IR (KBr): ν<sup>-</sup> = 3244 (NH), 1618 cm<sup>-1</sup> (CO); elemental analysis calcd (%) for C<sub>21</sub>H<sub>15</sub>FN<sub>4</sub>O<sub>3</sub> (MW: 390.37): C, 64.61; H, 3.87; N, 14.35; found: C, 64.70; H, 3.70; N, 14.10.

(5-Bromo-1-methyl-1H-indol-3-yl)[3-(5-fluoro-1H-indol-3-yl)-1,2,4-oxadiazol-5-yl]methanone (**1p**). *R*<sub>f</sub> = 0.67 (CH<sub>2</sub>Cl<sub>2</sub>/EtOAc 7:3); yellow solid; yield: 59%; mp: 280 °C (dec.); <sup>1</sup>H NMR (200 MHz, [D<sub>6</sub>]DMSO) δ:

4.03 (s, 3H, CH<sub>3</sub>), 7.14 (td,  $J=9.1, 9.1, 2.6$  Hz, 1H, H-6'), 7.53-7.76 (m, 4H, H-6, H-7, H-7' and H-4'), 8.44-8.49 (m, 2H, H-4 and H-2'), 9.13 (s, 1H, H-2), 12.18 (s, 1H, NH); <sup>13</sup>C NMR (50 MHz, [D<sub>6</sub>]DMSO) δ: 33.9 (q), 99.5 (d), 102.1 (d,  $J_{C7a-F}=4.5$  Hz), 105.2 (d,  $J_{C4-F}=25.1$  Hz), 111.0 (d,  $J_{C6-F}=26.6$  Hz), 112.0 (s), 113.7 (d,  $J_{C7-F}=9.2$  Hz), 116.4 (s), 123.6 (d), 124.6 (d,  $J_{C3a-F}=11.1$  Hz), 126.6 (d), 128.1 (s), 131.6 (d), 133.5 (s), 136.3 (s), 143.2 (d), 158.0 (d,  $J_{C5-F}=234.4$  Hz), 165.1 (s), 169.3 (s), 170.2 (s); IR (KBr):  $\nu=3310$  (NH), 1592 cm<sup>-1</sup> (CO); elemental analysis calcd (%) for C<sub>20</sub>H<sub>12</sub>BrFN<sub>4</sub>O<sub>2</sub> (MW: 439.24): C, 54.69; H, 2.75; N, 12.76; found: C, 54.80; H, 2.81; N, 12.60.

## Biology

### Drugs and Chemicals

Each compound was initially dissolved in dimethyl sulfoxide (DMSO), in order to obtain 10 mM stock solution, stored at +4 °C, which was then diluted in complete culture medium immediately before use at the appropriate concentration. The medium, Foetal Bovine Serum (FBS), penicillin and streptomycin were from Gibco (Gaithersburg, MD, USA).

### Cell culture

For the *in vitro* experiments in PDAC cell lines, we selected three models which are representative of primary (Panc-1) and metastatic (SUIT-2 and Capan-1) PDAC as well as of epithelial (SUIT-2 and Capan-1) and mesenchymal (Panc-1) phenotypes.

SUIT-2 is a cell line derived from a metastatic liver tumour of human pancreatic carcinoma. SUIT-2 cell line produces and releases at least two tumour markers, carcinoembryonic antigen and carbohydrate antigen 19-9.<sup>[44]</sup> Cells were cultured in Roswell Park Memorial Institute (RPMI) supplemented with 10% FBS and 1% Pen/Strep in T-75 flasks.

Capan-1 cells are adherent epithelial-like cells derived from a liver metastasis of a pancreatic adenocarcinoma that grown in tissue culture appeared as large epithelial-like mucin-producing cells.<sup>[45,46]</sup> Cells were cultured in Dulbecco's Modified Eagle Medium (DMEM) supplemented with 10% foetal bovine serum and 20 mM (1%) HEPES in T-75 flasks.

Panc-1 is an epithelioid carcinoma attached cell line, that is commonly used as an *in vitro* model to study pancreatic ductal adenocarcinoma carcinogenesis and tumour therapies, especially in light of the presence of the SSTR2 receptors, which have been proposed as potential prognostic markers in pancreatic cancer.<sup>[47,48]</sup> Panc-1 cells were cultured in Dulbecco's Modified Eagle Medium (DMEM) supplemented with 10% fetal bovine serum and 20 mM (1%) HEPES in T-75 flasks.

hTERT-HPNE is a human pancreatic duct epithelial-like cell line. Cells were obtained from the American Type Culture Collection (ATCC, Manassas, VA) and cultured in RPMI-1640, supplemented with 10% heat-inactivated-FBS, 10 ng/ml human recombinant EGF and 1% streptomycin/penicillin at 37 °C, in T-75 flasks.

The cell lines were routinely tested for Mycoplasma, while their authentication was performed by short tandem repeat-polymerase chain reaction at BaseClear (Leiden, the Netherlands).

### Viability assay *in vitro*

Cytotoxic activity of the topsentin derivatives **1b**, **1c**, **1i**, **1j** and **1l** on pancreatic cancer cells (SUIT-2, Capan-1 and Panc-1) and on non-neoplastic pancreatic cells (HPNE) was determined by the

sulforhodamine B (SRB) chemosensitivity assay, as described previously.<sup>[49]</sup>

Cells were plated in 96-well flat-bottom plates at final concentrations ranging from 3000–5000 cells/well in 100 μL of medium. After a 24 hours pre-incubation period, cells were treated with the compounds at nine screening concentrations (from 0.1 μM to 40 μM) in triplicate and incubated at 37 °C for 72 hours. After the treatment, cells were fixed with 25 μL of cold 50% trichloroacetic acid (TCA) for each well and incubated at 4 °C for 1 hour. Afterwards plates were washed five times with demi-water and air dried overnight. Then, the plates were stained with 50 μL of 0.4% SRB solution in 1% acetic acid for 15 minutes. The excess stain was rinsed off by placing the plates under running 1% acetic acid and allowed to dry at room temperature for overnight. SRB staining was rinsed with 150 μL tris(hydroxymethyl)aminomethane solution pH= 8.8 (TRIS-base), and the optical density (OD) was read at 492 nm. Each assay was performed in triplicate and assays were repeated at least three times. The comparison of the average optical density of the growth in control wells with that in the sample wells allowed estimating the percentage of cell growth, using the following equation:

$$\% \text{ Cell Growth} = \frac{(\text{mean OD}_{\text{compound}} - \text{mean OD}_{\text{day zero plate}})}{(\text{mean OD}_{\text{cells}} - \text{mean OD}_{\text{day zero plate}})} \times 100$$

The results obtained were adjusted by the day zero plate (wells containing cells growing for only 24 hours) and normalized by the control cells (wells with untreated cells) to obtain the rate of viable cells.

### Cell cycle analysis

Cell cycle modulation was analyzed by flow cytometry, as described previously.<sup>[49]</sup> Cells ( $2.5 \times 10^5$  cells/flask) were seeded in T25 cell flasks. After overnight incubation at 37 °C, the cells were treated with the compounds **1b**, **1c**, **1l**, at two concentrations (i.e., 2 μM and 5 μM for **1b** and 5 μM and 10 μM for **1c** and **1l**), and incubated for 24 hours. Drug concentrations were chosen on the basis of the respective EC<sub>50</sub> values. After treatment, the cells were harvested by trypsinization (0.5 mL/flask of trypsin-EDTA), incubated until the cells detached from the bottom of the flask and collected using the same medium used for the culture. The samples were then centrifuged in order to form a pellet (5 minutes at 1200 rpm). Finally, these pellets were fixed in ice-cold 70% ethanol, washed twice with phosphate-buffered saline (PBS) and incubated for 30 minutes at 37 °C with 50 μL of RNase (100 μg/mL) followed by incubation with 200 μL of propidium iodide solution (PI, 50 μg/mL). The cycle analysis was performed on the FACS Calibur instrument (Becton Dickinson, San José, CA). Data analysis was carried out with FACSDiva software (Becton Dickinson), while cell cycle distribution was determined using Modfit software (Verity-Software, Topsham, ME).

### Cell apoptosis analysis

Apoptosis induction was evaluated with by detection of the externalization of phosphatidylserine to the cell surface using the double staining with annexin V/7-AAD. To perform this assay, cells ( $2.0 \times 10^5$  cells/flask) were seeded in T25 flasks. After overnight incubation at 37 °C, the cells were treated with compounds **1b**, **1c**, **1l** at two concentrations (i.e. 2 μM and 5 μM for **1b**, and 5 μM and 10 μM for **1c** as well as for **1l**) and incubated for another 24 hours. Cells recovered from cultures were trypsinized and resuspended in fresh medium. Cells were then stained by the addition of 7AAD and

annexin V. In particular, a volume of 2.5  $\mu\text{L}$  of 7-AAD (Calbiochem, San Diego, CA) was added to 100  $\mu\text{L}$  of cell suspension. The samples were incubated in the dark at room temperature for 15 minutes. Each sample was washed in 3 mL of PBS, supplemented with 0.1% HSA and azide, and pelleted by centrifugation. Staining of the apoptotic cells was performed by incubating the cells with annexin V-FITC in annexin buffer (1:1000) for 15 minutes on ice. The samples were analyzed with a FACScan and data analysis was carried out with FACSDiva software (Becton Dickinson).

### Wound healing assay

Cell migration was assessed using a wound healing assay, as described previously.<sup>[50]</sup> A total of  $5 \times 10^4$  cells/well were seeded in a 96-well plate, to form confluent monolayer. Gaps or scratch were created in confluent cell layers using the sterile scratch tool (Figure 6c). The detached cell following scratch induction were removed and new medium was added to the wells. Cells were next treated with two concentrations of each compound (i.e. 2  $\mu\text{M}$  and 5  $\mu\text{M}$  for **1b** and 5  $\mu\text{M}$  and 10  $\mu\text{M}$  for **1c** and **1l**). Cells growing in complete medium were maintained at 37 °C with a supply of 5%  $\text{CO}_2$ /95% air atmosphere and 100% relative humidity. The wound closure was monitored by phase-contrast microscopy and photographed at the 0th, 4th, 8th, 20th and 24th hour. Pictures of the plates were taken using the Universal Grab 6.3 software (DCILabs) from a computer connected to a Leica microscope with a JAI TMC-1327 camera.

The percentage of migration was calculated using the following equation:

$$\% \text{ Migration} = \frac{(\text{Wound width at } t = 0 - \text{Wound width at } t = X)}{(\text{Wound width at } t = 0)} \times 100$$

### Gene expression analysis

In order to evaluate the capability of epithelial to mesenchymal transition (EMT) modulation by the new most active oxadiazole compounds **1b** and **1l**, we determined the gene expression of key EMT determinants by Real-Time PCR analysis in Panc-1 and Capan-1 cells.

Cells ( $3 \times 10^5$  cells/well) were seeded in a 6-well plate and treated with compounds for 24 hours. Cells were then harvested by 250  $\mu\text{L}$  of Trizol reagent and collected in a new eppendorf tube. Total RNA was extracted by adding 50  $\mu\text{L}$  chloroform to each sample, shaking vigorously and spinning 10 minutes at 12000 RPM at 4 °C, after 3 minutes of incubation at room temperature. After obtaining a lysate from each sample, the upper aqueous phase containing RNA was collected and washed with isopropanol and 70% ethanol. The pellet was resuspended in nuclease free water and the amount of nucleic acid was determined through NanoDrop technology.

Afterwards, reverse transcription (RT) reactions to produce cDNA from RNA for RT-PCR were conducted using M-MuLV RNase H<sup>+</sup> reverse transcriptase enzyme, Reverse Transcription buffer 2X, including dNTP mix and  $\text{MgCl}_2$ , and random hexamers primer (DyNAmo™ cDNA Synthesis Kit). cDNA was synthesised from 7  $\mu\text{L}$  of RNA at concentration of 143 ng/mL in a 13  $\mu\text{L}$  reaction volume (10  $\mu\text{L}$  of RT buffer, 1  $\mu\text{L}$  of random hexamer primer and 2  $\mu\text{L}$  of Reverse Transcriptase). The cDNA synthesis reactions were initiated with a primer extension step at 25 °C for 10 minutes, followed by cDNA synthesis at 37 °C for 30 minutes, termination at 85 °C for 5 minutes and sample cooling at 4 °C.

Finally, RT-PCR reactions were performed using the commercial kit TaqMan® Universal PCR Master Mix. Amplification mixtures, set up in a final volume of 25  $\mu\text{L}$ , contained 12.5  $\mu\text{L}$  of Universal Master Mix 2X (AmpliAq Gold DNA Polymerase, dNTPs with dUTP, passive reference, and optimized buffer components), 1  $\mu\text{L}$  of Primers and TaqMan® probe, 6.5  $\mu\text{L}$  of  $\text{H}_2\text{O}$  and 5  $\mu\text{L}$  of cDNA sample. RT-PCR assays were carried out in a GeneAmp 5700 Sequence Detection System programmed to hold at 50 °C for 30 minutes, to hold at 95 °C for 10 minutes, and to complete 45 cycles of 95 °C for 15 minutes and 50 °C for 1 minute. The gene expression profiling was determined using the Sequence Detection System (SDS) software, as described previously.<sup>[51]</sup>

### Analysis of the activity of MMP9 by gelatine zymography

The activity of MMP9 was evaluated by gelatine zymography, as described.<sup>[52]</sup> Panc-1 and Capan-1 cells ( $10^6$ ) were seeded in Petri dishes and incubated with serum-free medium for 24 hours, with or without the most promising compounds **1b** and **1l** at 2 and 5  $\mu\text{M}$ . Medium was harvested and centrifuged in order to remove cellular debris. The media were then mixed with SDS-PAGE buffer 4X without reducing agent and underwent electrophoresis in 10% polyacrylamide gel containing 1 mg/mL gelatine. After 1 hour, the gel was exposed to renaturing buffer and finally incubated with developing buffer. The staining was then performed using 0.25% Coomassie Brilliant Blue R-250 solution and the areas of protease activity were detected as clear bands and the activity of MMP9 was assessed by using ImageJ software (National Institutes of Health, Bethesda, MD, US).

### PathScan intracellular signaling array

The fluorescent PathScan sandwich ELISA was purchased from Cell Signaling Technology (Leiden, Netherlands) and used according to manufacturer's instructions, as described previously.<sup>[53]</sup> The Panc-1 cells were seeded and treated for 24 hours and lysed in lysis buffer with 1 mM PMSF. The glass slide was blocked and the lysate was added to the wells. The slide was washed thoroughly and incubated with the detection antibody cocktail. The fluorescent signal was determined using the ArrayVision software, which measured the pixel intensity.

### Enzyme-linked immunosorbent assay (ELISA) for phosphorylated GSK3 $\beta$ kinase

The phospho-GSK3 $\beta$  levels at serine residue 9 and at tyrosine residue 216 were detected and quantified using Enzyme-Linked Immunosorbent Assay (ELISA, Invitrogen™ phospho-GSK3 beta (Ser9) InstantOne Kit, Catalog Number: 85-86172 and Biomatik Phospho-GSK3 (Tyr216) kit, Cat#EKA50974) according to the manufacturer's protocols. Supernatants from Panc-1, cells were evaluated after 24 hours from the treatment with the selected compounds **1b** and **1l** at 5  $\mu\text{M}$  concentration. The absorbance was read at 450 nm. We performed a parallel ELISA test using the inhibitor enzastaurin (5  $\mu\text{M}$ ), as described previously.<sup>[54]</sup> This drug reduced the phosphorylation of 65%, supporting the use of this method in order to check the inhibition of phospho-GSK3 $\beta$ .

### GSK3 $\beta$ kinase assay

The inhibitory activity on GSK3 $\beta$  was evaluated by using the ADP-Glo™ Kinase Assay kit from Promega (Promega Corporation, Madison, WI 53711, USA). The assay was performed in non-treated 384-well plates as previously describe,<sup>[55]</sup> using a volume of 2  $\mu\text{L}$  of

recombinant human GSK3 $\beta$  and 2  $\mu$ L of substrate/ATP mix, in presence of serial dilutions of each compound (**1b**, **1c**, **1i**, **1j** and **1l**). Kinase was incubated with the test compounds for 10 min at rt and the reaction was then started with the addition of substrate/ATP and run for 60 min at rt. After the addition of ADP-Glo™ reagent (5  $\mu$ L, for 40 minutes incubation) and kinase detection reagent (10  $\mu$ L, for 30 minutes incubation), the luminescence was measured with an integration time of 0.5–1 second. Raw data were normalized to the values of control wells and plotted using GraphPad Prism 8.

### Molecular modeling

The X-ray crystal structure of GSK-3 $\beta$  (PDB ID 1UV5)<sup>[40]</sup> was retrieved from the RCSB Protein Data Bank (<http://www.rcsb.org>). Schrödinger's Protein Preparation Wizard of the Prime module was used for protein structure refinements (Prime, Schrödinger, LLC, New York, NY, 2017). In the pre-process phase, hydrogen atoms were added and bond orders were assigned, missing loops were filled according to the amino acid sequence. In the refinement phase the hydrogen bond network was restored using the H-bond assignment option, which was followed by a restrained minimization (converged heavy atoms to RMSD: 0.3 Å) with OPLS\_2003 force field.

Schrödinger's Maestro was used to visualize interactions between binding site and inhibitors (Maestro, 11.1 version, Schrödinger, LLC, New York, NY, 2017). Structures of compounds **1b** and **1l** were drawn manually, 2D structures were optimized with Schrödinger's LigPrep module with standard settings using the OPLS\_2003 forcefield (LigPrep, Schrödinger, LLC, New York, NY, 2017). Compounds were docked with Schrödinger's Glide software package (Glide, Schrödinger, LLC, New York, NY, 2017). In the grid generation phase, the position of the grid box was determined by the co-crystallized ligand: the center of the docking box was fixed on the center of the inhibitor. The size of the box was 20  $\times$  20  $\times$  20 Å (the inner box was 10  $\times$  10  $\times$  10 Å). The standard precision mode (SP) and standard settings (Van der Waals Radius and Charge Scaling) were used for calculations. Moreover, the crystallized ligand 6-bromindirubin was redocked with the aim to evaluate the ability of SP protocol to reproduce the experimental conformation.

### Statistics

All the SRB, PCR, zymography and ELISA assays were carried out in triplicate and repeated at least three times, whereas the percentages of cell migration were calculated taking into account at least six scratch areas. The data was evaluated using the GraphPad Prism v. 5 software (GraphPad Software, San Diego, CA). Data was expressed as mean values  $\pm$  SEM and analyzed by the Student t test. *P* values < 0.05 were considered significant (\*).

### Acknowledgements

This work was partially supported by the following grants: CCA Foundation 2015 and 2018 grants, KWF Dutch Cancer Society grants (KWF project#11957), AIRC/Start-Up grant (to E.G.), PRIN2017, Prot.No.2017E84AA4 and European Union 2014-2020 PON Ricerca e Innovazione grant from the Italian Ministry of Education, University and Research, entitled "PROGEMA-Processi Green per l'Estrazione di Principi Attivi e la Depurazione di Matrici di Scarto e Non" (ARS01\_00432) to P.D. The Authors would like to

thank Professor A Griffioen (Angiogenesis group, Department Medical Oncology, VUmc, Amsterdam VUmc, Amsterdam) for the migration station used to perform wound healing assays, and the members of the Drug Discovery Committee of the EORTC-PAMM group for the useful discussion and support.

### Conflict of Interest

The authors declare no conflict of interest.

**Keywords:** 1,2,4-oxadiazole topsentin analogs · inhibition of migration · GSK3 $\beta$  kinase · PDAC antiproliferative activity · proapoptotic activity

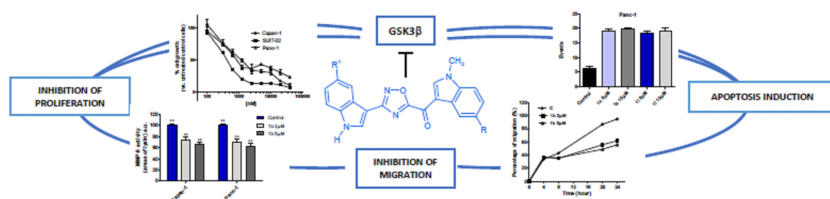
- [1] D. J. Newman, G. M. Cragg, *J. Nat. Prod.* **2016**, *79* (3), 629–661.
- [2] U. Lindequist, *Biomol. Ther. (Seoul)*. **2016**, *24* (6), 561–571.
- [3] S. Sakemi, H. H. Sun, *J. Org. Chem.* **1991**, *56*, 4304–4307.
- [4] A. Carbone, B. Parrino, P. Barraja, V. Spanò, G. Cirrincione, P. Diana, A. Maier, G. Kelter, H. H. Fiebig, *Mar. Drugs* **2013**, *11* (3), 643–654.
- [5] P. Diana, A. Carbone, P. Barraja, A. Martorana, O. Gia, L. DallaVia, G. Cirrincione, *Bioorg. Med. Chem. Lett.* **2007**, *17* (22), 6134–6137.
- [6] P. Diana, A. Carbone, P. Barraja, A. Montalbano, A. Martorana, G. Dattolo, L. DallaVia, G. Cirrincione, *Bioorg. Med. Chem. Lett.* **2007**, *17*, 2342–2346.
- [7] P. Diana, A. Carbone, P. Barraja, G. Kelter, H.-H. Fiebig, G. Cirrincione, *Bioorg. Med. Chem.* **2010**, *18*, 4524–4529.
- [8] V. Spanò, A. Attanzio, S. Cascioferro, A. Carbone, A. Montalbano, P. Barraja, L. Tesoriere, G. Cirrincione, P. Diana, B. Parrino, *Mar. Drugs* **2016**, *14*, 226.
- [9] B. Parrino, A. Carbone, G. Di Vita, C. Ciancimino, A. Attanzio, A. Montalbano, P. Barraja, L. Tesoriere, M. A. Livrea, P. Diana, G. Cirrincione, *Mar. Drugs* **2015**, *13*, 1901–1924.
- [10] A. Carbone, B. Parrino, G. Di Vita, A. Attanzio, V. Spanò, A. Montalbano, P. Barraja, L. Tesoriere, M. A. Livrea, P. Diana, G. Cirrincione, *Mar. Drugs* **2015**, *13*, 460–492.
- [11] A. Carbone, M. Pennati, P. Barraja, A. Montalbano, B. Parrino, V. Spano, A. Lopergolo, S. Sbarra, V. Doldi, N. Zaffaroni, G. Cirrincione, P. Diana, *Curr. Med. Chem.* **2014**, *21* (14), 1654.
- [12] P. Diana, A. Carbone, P. Barraja, A. Montalbano, B. Parrino, A. Lopergolo, M. Pennati, N. Zaffaroni, *ChemMedChem* **2011**, *6*, 1300–1309.
- [13] A. Carbone, M. Pennati, B. Parrino, A. Lopergolo, P. Barraja, A. Montalbano, V. Spanò, S. Sbarra, V. Doldi, M. De Cesare, G. Cirrincione, P. Diana, N. Zaffaroni, *J. Med. Chem.* **2013**, *56* (17), 7060–7072.
- [14] B. Bao, Q. Sun, X. Yao, J. Hong, C. O. Lee, C. J. Sim, K. S. Im, J. H. Jung, *J. Nat. Prod.* **2005**, *68* (5), 711–715.
- [15] S. Tsujii, K. L. Rinehart, S. P. Gunasekera, S. S. Cross, M. S. Lui, S. A. Pomponi, M. Cristina Diaz, Y. Kashman, *J. Org. Chem.* **1988**, *53* (23), 5446–5453.
- [16] K.-B. Oh, W. Mar, S. Kim, J.-Y. Kim, T.-H. Lee, J.-G. Kim, D. Shin, C. J. Sim, J. Shin, *Biol. Pharm. Bull.* **2006**, *29* (3), 570–573.
- [17] J. Shin, Y. Seo, K. W. Cho, J. R. Rho, C. J. Sim, *J. Nat. Prod.* **1999**, *62* (4), 647–649.
- [18] B. Parrino, D. Schillaci, I. Carnevale, E. Giovannetti, P. Diana, G. Cirrincione, S. Cascioferro, *Eur. J. Med. Chem.* **2019**, *161*, 154–178.
- [19] P. Diana, A. Stagno, P. Barraja, A. Montalbano, A. Carbone, B. Parrino, G. Cirrincione, *Tetrahedron* **2011**, *67* (19), 3374–3379.
- [20] S. Cascioferro, B. Parrino, G. Li Petri, M. G. Cusimano, D. Schillaci, V. Di Sarno, S. Musella, E. Giovannetti, G. Cirrincione, P. Diana, *Eur. J. Med. Chem.* **2019**, *167*, 200–210.
- [21] S. Cascioferro, G. Li Petri, B. Parrino, B. El Hassouni, D. Carbone, V. Arizza, U. Perricone, A. Padova, N. Funel, G. J. Peters, G. Cirrincione, E. Giovannetti, P. Diana, *Molecules* **2020**, *25*, 329.
- [22] G. Li Petri, S. Cascioferro, B. El Hassouni, D. Carbone, B. Parrino, G. Cirrincione, G. J. Peters, P. Diana, E. Giovannetti, *Anticancer Res.* **2019**, *39*, 3615–3620.
- [23] B. Parrino, A. Carbone, V. Spanò, A. Montalbano, D. Giallombardo, P. Barraja, A. Attanzio, L. Tesoriere, C. Sissi, M. Palumbo, G. Cirrincione, P. Diana, *Eur. J. Med. Chem.* **2015**, *94*, 367–377.

- [24] B. Parrino, A. Carbone, C. Ciancimino, V. Spanò, A. Montalbano, P. Barraja, G. Cirrincione, P. Diana, C. Sissi, M. Palumbo, O. Pinato, M. Pennati, G. Beretta, M. Folini, P. Matyus, B. Balogh, N. Zaffaroni, *Eur. J. Med. Chem.* **2015**, *94*, 149–162.
- [25] N. Kerru, L. Gummidi, S. Maddila, K. K. Gangu, S. B. Jonnalagadda, *Molecules* **2020**, *25* (8).
- [26] D. Kumar, G. Patel, A. K. Chavers, K.-H. Chang, K. Shah, *Eur. J. Med. Chem.* **2011**, *46* (7), 3085–3092.
- [27] H.-Z. Zhang, S. Kasibhatla, J. Kuemmerle, W. Kemnitzer, K. Ollis-Mason, L. Qiu, C. Crogan-Grundy, B. Tseng, J. Drewe, S. X. Cai, *J. Med. Chem.* **2005**, *48* (16), 5215–5223.
- [28] M. Krasavin, A. V. Sosnov, R. Karapetian, I. Konstantinov, O. Soldatkina, E. Godovykh, F. Zubkov, R. Bai, E. Hamel, A. A. Gakh, *Bioorg. Med. Chem. Lett.* **2014**, *24* (18), 4477–4481.
- [29] S. Cascioferro, A. Attanzio, V. Di Sarno, S. Musella, L. Tesoriere, G. Cirrincione, P. Diana, B. Parrino, *Mar. Drugs* **2019**, *17*, 35.
- [30] A. Carbone, B. Parrino, M. G. Cusimano, V. Spanò, A. Montalbano, P. Barraja, D. Schillaci, G. Cirrincione, P. Diana, S. Cascioferro, *Mar. Drugs* **2018**, *16* (8), 274–289.
- [31] L. Zhang, Q. Wen, J. Jin, C. Wang, P. Lu, Y. Wang, *Tetrahedron* **2013**, *69* (21), 4236–4240.
- [32] B. Parrino, A. Attanzio, V. Spanò, S. Cascioferro, A. Montalbano, P. Barraja, L. Tesoriere, P. Diana, G. Cirrincione, A. Carbone, *Eur. J. Med. Chem.* **2017**, *138*, 371–383.
- [33] E. Valeur, M. Bradley, *Chem. Soc. Rev.* **2009**, *38* (2), 606–631.
- [34] V. J. Bhagwandin, J. M. Bishop, W. E. Wright, J. W. Shay, *PLoS One* **2016**, *11* (2), 1–16.
- [35] G. A. Lee, K. A. Hwang, *Toxin Rev.* **2016**, *8* (6), 1–17.
- [36] N. Gavert, A. Ben-Ze'ev, *Trends Mol. Med.* **2008**, *14* (5), 199–209.
- [37] H. Hugo, M. L. Ackland, T. Blick, M. G. Lawrence, J. A. Clements, E. D. Williams, E. W. Thompson, *J. Cell. Physiol.* **2007**, *213*, 374–383.
- [38] S. Peirò, M. Escriva, I. Puig, M. J. Barberà, N. Dave, N. Herranz, M. J. Larriba, M. Takkunen, C. Franci, A. Munoz, I. Virtanen, J. Baulida, A. G. Herreros, *Nucleic Acids Res.* **2006**, *34* (7), 2077–2084.
- [39] R. Bhat, Y. Xue, S. Berg, S. Hellberg, M. Ormo, Y. Nilsson, A.-C. Radesater, E. Jerning, P.-O. Markgren, T. Borgegård, M. Nylof, A. Gimenez-Cassina, F. Hernandez, J. J. Lucas, J. Diaz-Nido, J. Avila, *J. Biol. Chem.* **2003**, *278*, 45937–45945.
- [40] L. Meijer, A.-L. Skaltsounis, P. Magiatis, P. Polychronopoulos, M. Knockaert, M. Leost, X. P. Ryan, C. A. Vonica, A. Brivanlou, R. Dajani, C. Crovace, C. Tarricone, A. Musacchio, S. M. Roe, L. Pearl, P. Greengard, *Chem. Biol.* **2003**, *10* (12), 1255–1266.
- [41] F. Heider, T. Pantsar, M. Kudolo, F. Ansideri, A. De Simone, L. Pruccoli, T. Schneider, M. I. Goettert, A. Tarozzi, V. Andrisano, S. A. Laufer, P. Koch, *ACS Med. Chem. Lett.* **2019**, *10* (10), 1407–1414.
- [42] H. Park, Y. Shin, J. Kim, S. Hong, *J. Med. Chem.* **2016**, *59* (19), 9018–9034.
- [43] K. Lynch, W. Santos, WO 2016054261, **2016**; *Chem. Abstr.* **2016**, 164, 472549.
- [44] Y. Ikeda, M. Ezakv, I. Hayashv, D. Yasuda, K. Nakayama, *Jpn. J. Cancer Res.* **1990**, *81*, 987–993.
- [45] P. Skehan, S. J. Friedman, *Vitr. Cell. Dev. Biol.* **2014**, *21* (5), 288–290.
- [46] M. Lieber, J. Mazzetta, W. Nelson-Rees, M. Kaplan, G. Todaro, *Int. J. Cancer* **1975**, *15* (5), 741–747.
- [47] R. Gradiz, H. C. Silv, L. Carvalho, M. F. Botelho, *Sci. Rep.* **2016**, No. February, 1–14.
- [48] M. Pilichowska, N. Kimura, M. Schindler, M. Kobari, *Endocr. Pathol.* **2001**, *12* (2), 147–155.
- [49] R. Sciarillo, A. Wojtuszkiewicz, I.E. Kooi, V.E. Gómez, U. Boggi, G. Jansen, G. J. Kaspers, J. Cloos, E. Giovannetti, *J. Visualization* **2016**, *118*, e54714.
- [50] E. Giovannetti, Q. Wang, A. Avan, N. Funel, T. Lagerweij, J.-H. Lee, V. Caretti, A. van der Velde, U. Boggi, Y. Wang, E. Vasile, G. J. Peters, T. Wurdinger, G. Giaccone, *J. Natl. Cancer Inst.* **2014**, *106* (1), djt346.
- [51] E. Giovannetti, P. A. Zucali, Y. G. Assaraf, L. G. Leon, K. Smid, C. Alecci, F. Giancola, A. Destro, L. Gianoncelli, E. Lorenzi, M. Roncelli, A. Santoro, G. J. Peters, *Br. J. Cancer* **2011**, *105* (10), 1542–1553.
- [52] S. Cascioferro, G. Li Petri, B. Parrino, D. Carbone, N. Funel, C. Bergonzini, G. Mantini, H. Dekker, D. Geerke, G. J. Peters, G. Cirrincione, E. Giovannetti, P. Diana, *Eur. J. Med. Chem.* **2020**, *189*, 112088.
- [53] N. Van Der Steen, A. Leonetti, K. Keller, H. Dekker, N. Funel, F. Lardon, R. Ruijtenbeek, M. Tiseo, C. Rolfo, P. Pauwels, G. J. Peters, *E. Biochem. Pharmacol.* **2019**, *166*, 128–138.
- [54] E. Giovannetti, R. Honeywell, A. R. Hanauske, C. Tekle, B. Kuenen, J. Sigmond, G. Giaccone, G. J. Peters, *Curr. Drug Targets* **2010**, *11* (1), 12–28.
- [55] F. Heider, F. Ansideri, R. Tesch, T. Pantsar, U. Haun, E. Doring, M. Kudolo, A. Poso, W. Albrecht, S. A. Laufer, P. Koch, *Eur. J. Med. Chem.* **2019**, *175*, 309–329.

Manuscript received: September 21, 2020

Version of record online: ■■■, ■■■■

## FULL PAPERS



**Tip-topsentins!** 1,2,4-Oxadiazole topsentin analogs were efficiently synthesized. Five derivatives showed high antiproliferative activity against pancreatic cancer cells, with pro-apoptotic effects. The compounds remarkably reduced the migration of

Capan-1 cells, with a decrease in the activity of MMP-9 protein levels. The most active oxadiazoles confined viable cells in G<sub>2</sub>/M phase and markedly inhibited the kinase activity of GSK3 $\beta$  *in vitro*.

Dr. D. Carbone, Dr. B. Parrino, Dr. S. Cascioferro, C. Pecoraro, Prof. E. Giovannetti, Dr. V. Di Sarno, Dr. S. Musella, Dr. G. Auriemma, Prof. G. Cirrincione, Prof. P. Diana\*

1 – 19

**1,2,4-Oxadiazole Topsentin Analogs with Antiproliferative Activity against Pancreatic Cancer Cells, Targeting GSK3 $\beta$  Kinase**

